journal of the mechanical behavior of biomedical materials 134 (2022) 105371

Contents lists available at ScienceDirect

Journal of the Mechanical Behavior of Biomedical Materials

journal homepage: www.elsevier.com/locate/jmbbm

Research paper

Microstructure and mechanics of the bovine trachea: Layer specific investigations through SHG imaging and biaxial testing

Venkat Ayyalasomayajula *, Bjørn Skallerud

Department of Structural Engineering, Norwegian University of Science and Technology, Trondheim, Norway

ARTICLE INFO

Keywords:
Collagen fibers
Muscle fibers
Trachea
Constitutive modeling

ABSTRACT

The trachea is a complex tissue made up of hyaline cartilage, fibrous tissue, and muscle fibers. Currently, the knowledge of microscopic structural organization of these components and their role in determining the tissue's mechanical response is very limited. The purpose of this study is to provide data on the microstructure of the tracheal components and its influence on tissue's mechanical response. Five bovine tracheae were used in this study. Adventitia, cartilage, mucosa/submucosa, and trachealis muscle layers were methodically cut out from the whole tissue. Second-harmonic generation(SHG) via multi-photon microscopy (MPM) enabled imaging of collagen fibers and muscle fibers. Simultaneously, a planar biaxial test rig was used to record the mechanical behavior of each layer. In total 60 samples were tested and analyzed. Fiber architecture in the adventitia and mucosa/submucosa layer showed high degree of anisotropy with the mean fiber angle varying from sample to sample. The trachealis muscle displayed neat layers of fibers organized in the longitudinal direction. The cartilage also displayed a structure of thick mesh-work of collagen type II organized predominantly towards the circumferential direction. Further, mechanical testing demonstrated the anisotropic nature of the tissue components. The cartilage was identified as the stiffest component for strain level < 20% and hence the primary load bearing component. The other three layers displayed a non-linear mechanical response which could be explained by the structure and organization of their fibers. This study is useful in enhancing the utilization of structurally motivated material models for predicting tracheal overall mechanical response.

1. Introduction

The trachea is a highly deformable structure composed of four different layers: adventitial layer, cartilaginous layer, mucosa/submucosa layer, and the trachealis muscle. The primary function of the trachea is to provide necessary mechanical compliance for changes in intraluminal pressure during breathing, coughing, and swallowing (Minnich and Mathisen, 2007).

There are two primary disorders that affect the trachea: tracheal stenosis and tracheomalacia. Stenosis, even though rare, is a potentially life threatening condition which narrows the tracheal lumen and causes severe difficulty in breathing (Ho and Koltai, 2008; Benjamin et al., 1981). Tracheomalacia on the other hand is a result of biomechanical degradation of longitudinal fibers or cartilage (Fraga et al., 2016), which makes the trachea more susceptible to collapse under physiological pressure changes (Hysinger and Panitch, 2016). Current treatment methods such as replacing the diseased region with stents (Kojima and Vacanti, 2014) and prosthetic materials (Kojima et al., 2003) often do not mimic the properties of native tissues. Tracheal tissue engineering has showed great promise in developing a clinically useful tissue-engineered replacement (Ott et al., 2011). However, current methods rely solely on cartilage reconstruction. There is a need to construct a composite tissue that also incorporates the other layers as suggested by Orlando et al. (2011), which poses the question on structure and composition of all the layers in order to mimic its behavior.

Each layer of the trachea at the micro-meter scale is composed of a network of various types of fibers, in particular collagen and muscle fibers. The role of fiber networks in soft-tissue's mechanical behavior has been adequately substantiated through experimental (Keyes et al., 2011; Krasny et al., 2018; Meador et al., 2020) and numerical studies (Giraudet et al., 2022; Terzolo et al., 2022; Frank et al., 2019). Understanding structure-function relationship is of paramount importance in developing tissue-engineered substitutes in order to emulate native tissue's mechanical behavior, especially in the case of fibrous bio-materials (D'Amore et al., 2014).

Several studies have examined the histology of the trachea in animals (Butler et al., 2014), in human subjects (Trabelsi et al., 2010),

* Corresponding author.
E-mail address: radhakrishna300792@gmail.com (V. Ayyalasomayajula).

https://doi.org/10.1016/j.jmbbm.2022.105371
Received 6 April 2022; Received in revised form 20 June 2022; Accepted 9 July 2022
Available online 14 July 2022

and tissue-engineered samples (Liu et al., 2010). While histology imaging reveals a lot of information on the layered structure and microstructural constituents of the tissue, it does not reveal much about their morphological organization. With the advent of more powerful optical imaging techniques such as multi-photon microscopy, microscopic investigations of fiber architecture in tissues could be achieved thanks to second harmonic generation(SHG) without any staining or fixation. SHG imaging applied to the trachea is often limited to the cartilaginous layer (Brockbank et al., 2008), used for analyzing the difference in fiber architecture in fibrous and hyaline cartilage (Zhu et al., 2016). To the best of our knowledge, only a handful of studies focused on quantification of the whole tissue's microstructure (Thiberville et al., 2007). In Ansari et al. (2015) the imaging volume of 128 μm in plane and 40 μm in depth was obtained via OCT. This gives detailed information of the micro-structure and could be improved by SHG in this study with an in-plane field of view of 465 μm and scan depth more than 200 μm. An interesting study that explores the 3-d architecture of the vasculature in the tissue using optical clearing (Sun et al., 2021), does not however shed light on any constituents that influence the mechanics of the tissue.

Characterizing the native tissue also involves quantifying its mechanical behavior. Early efforts in this direction include the characterization of pressure–volume relationships of the whole tissue at various physiological pressure levels in animals (Mortola and Sant'Ambrogio, 1979) and human tissue (Croteau and Cook, 1961). One particular study emphasized recording the mechanical response at different phases of development (Bhutani et al., 1981), underlining the importance of complex mechanobiological interactions leading to an alteration of the biomechanical behavior. As stated earlier, histology imaging led to the realization of trachea being a multi-layered structure, which prompted the need to mechanically characterize each layer individually. Tracheal cartilage has been extensively studied under uniaxial tension as its believed to be the main component for mechanical stability (Safshekan et al., 2017). Layer specific tests have gained traction with the most recent and the largest study to date conducted by Safshekan (2016) involving 30 human samples tested in uniaxial tension, suggesting material models for cartilage, adventitia, and the trachealis muscle. However, they do not take into consideration any directional dependence of the tissue's mechanical response (eg.: circumferential vs longitudinal) and provide only phenomenological material models that disregard the influence of microstructure on mechanical behavior. A few notable studies that evaluate the anisotropic behavior of the tissue include (Teng et al., 2012; Eskandari et al., 2018). Despite their valuable contributions, uniaxial tests do not mimic the tissue's complex deformation behavior in-vivo. In humans, the trachea sustains up to 20% extension in the longitudinal direction (Kamel et al., 2009; Cinar et al., 2016), while it was measured to be up to 25% in guinea pigs (Amiri and Gabella, 1988). Simultaneously the trachea sustains dynamic pressure changes which deforms the tissue in-vivo in radial and circumferential directions (Boazak and Auguste, 2018; Balakrishnan et al., 2018; Robertson et al., 2011). This type of deformation behavior is better represented through biaxial testing.

Numerical models can be used to predict the mechanical state of the structure under physiological and supra-physiological loading conditions (Safshekan et al., 2020; Malvè et al., 2011). Such simulations are widely used in the biomedical field to aid surgeons with decision making (Perrin et al., 2015; Mimouni-Benabu et al., 2012) and in developing suitable tissue-engineered substitutes (Eichaker et al., 2018). However, the material models as suggested by above mentioned experimental studies either do not conduct adequate micro-structural investigations and accept perfectly orthogonal fiber families (Trabelsi et al., 2010) or employ phenomenological models that do no account for any structural information (Safshekan, 2016; Eskandari et al., 2019). This leads to difficulties in studying and predicting the behavior of diseased tissues where changes in physiology and pathology directly influence its behavior.

Therefore, the primary objective of this study is to bridge the gap in knowledge of relevant micro-structure morphology through thorough multi-photon microscopy (MPM) investigation and its stochastic quantification. Further, biaxial tension testing is utilized to mimic the tissue's in-vivo deformation behavior. The results help in understanding the complex non-linear and anisotropic nature of the tissue layers, while also providing a structure based description of tracheal mechanics. Structure based constitutive models are proposed and evaluated for each tracheal component based on the investigated microstructure morphology. The findings from this study enable the utilization of layer specific micro-structure morphology thereby enhancing numerical tools to better predict the tissue's behavior in health and disease.

2. Methods

Prepared tissue samples were subjected to multi-photon microscopy to record the SHG emission signal. The samples were also subjected to planar biaxial-tension tests to record their mechanical response. All the protocols utilized in this study are presented here. A small distinction is to be noted: from here on specimen refers to the whole trachea, where as sample refers to an excised section from the trachea. Multiple samples were excised from each specimen.

2.1. Sample preparation

The trachea of healthy cows (n = 5) were obtained from a local slaughterhouse. For each animal the whole upper airway system was transported to the laboratory within 2 h of it being sacrificed. In all cases, the whole trachea was dissected carefully and transferred to the freezer operating at −28 °C until the day of testing. On the day of testing, the tracheal tissue was first thawed in a phosphate buffer saline solution (PBS) at 4 °C for 2 h and then at room temperature for a another 2 h. The trachea was then cut open at the point where the cartilage ring meets the trachealis smooth muscle. The cartilage rings were then inverted (turned inside-out), and the exposed mucosa/submucosa layers were peeled off carefully. For ease of use, the mucosa/submucosa layer is referred to as mucosa from here on. The adventitial layer was also peeled off from the cartilage rings, which is more complicated to isolate as its loosely attached to the cartilage at several intersections. The excised layers of specimen 3 are shown in Fig. 1. The thickness of each separated layer along with the internal diameter of the trachea were measured at multiple locations using a caliper (0.01 mm). The average anatomical features of each specimen are presented in Table 1. It is to be noted that the trachea has some pre-stress in the load-free, which was not considered here. It could influence the reference configurations of the layers before and after peeling. For each tracheal layer along the cartilage rings, three samples were excised per specimen along the circumference. For the trachealis muscle, given the limited width, three samples were excised in close proximity to each other in no particular order.

2.2. Multi-photon microscopy

MPM images of the tissue layers were obtained using a second harmonic generation (SHG) setup, which consists of a mode-locked Ti:Sapphire laser(Chameleon Vision; Coherent, Santa Clara, CA) and an inverted optical microscope. The average excitation power at the sample was 40 mW with an excitation wavelength of 890 nm. The SHG signals were collected through 390 nm–480 nm bandpass filter by the objective and directed towards two external photo multiplier tube (PMT) detectors. A 25 × 1.95 NA water immersion objective (LUMFI; Olympus America) was used for all specimens, and each acquired image covered an area of 465 × 465 μm^2 integrated over two frames to improve the signal/noise ratio. The step size between slices was typically set at 0.5–5 μm depending on the thickness of the sample. The depth of the scan, which depended on the quality of the signal in response to the pulsed laser beam, covered a thickness of at least 200 μm for each layer, giving adequate information. The total scan time for a single z-stack was less than 30 min.

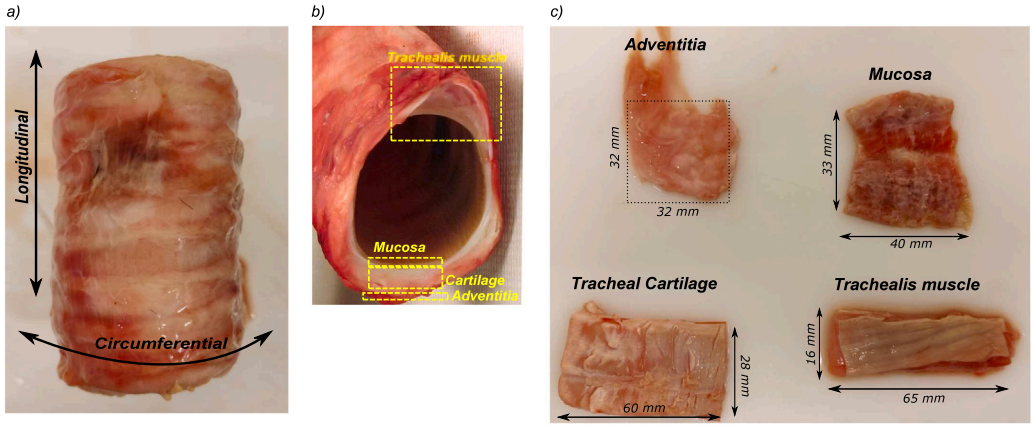

Fig. 1. Sample preparation from bovine trachea; (a) Excised whole trachea, (b) cross-section of the trachea depicting anatomical position of each component, (c) detached components of the trachea.

Table 1
Measured mean anatomy parameters for each layer of the trachea.

	Ex-vivo diameter (mm)	Thickness adventitia (mm)	Thickness cartilage (mm)	Thickness mucosa (mm)	Thickness trachealis muscle (mm)
Specimen 1	53.72 ± 3.77	0.67 ± 0.05	3.64 ± 0.04	1.68 ± 0.1	2.73 ± 0.05
Specimen 2	49.51 ± 1.46	0.62 ± 0.03	3.72 ± 0.07	1.74 ± 0.05	2.48 ± 0.03
Specimen 3	51.6 ± 2.28	0.78 ± 0.08	3.83 ± 0.11	1.95 ± 0.06	3.57 ± 0.03
Specimen 4	49.4 ± 1.53	0.72 ± 0.05	3.77 ± 0.08	1.82 ± 0.12	3.23 ± 0.07
Specimen 5	48.4 ± 2.14	0.68 ± 0.04	3.90 ± 0.06	1.90 ± 0.08	3.21 ± 0.04

2.3. Image processing and analysis

In order to assess structural organization of the fibrous structure, it was decided to focus on the orientation distribution of the collagen fibrous network in the longitudinal–circumferential plane. Taking into account previous observations from histology studies (Trabelsi et al., 2010), fibers exhibited practically planar organization in the longitudinal–circumferential plane. Hence, only the planar orientation distribution function of the collagen fibers was estimated. The image stacks representing the collagen (SHG signal) were analyzed to extract relevant quantitative information regarding orientation, fiber recruitment stretch, volume fraction.

A custom python script based on FFT principle was used to analyze the images. The application of this methodology was previously validated and reported in Polzer et al. (2013). Briefly, the images were pre-processed in ImageJ to reduce artifacts and improve the contrast of fibers. Following that, the images were analyzed resulting in an FFT spectrum. A 1° wedge-filter was used to extract the fiber orientations by summing up the amplitudes in each wedge. This resulted in a discrete distribution of amplitudes which was then averaged for the entire stack to compute the orientation histogram. The orientation distribution of fibers in the microstructure was then fit using a finite mixture of Von-Mises distributions given by Eqs. (1) and (2).

$$f(\theta\|\mu_i, a_i) = \frac{e^{a_i cos2(\theta-\mu_i)}}{\pi I_0(a_i)} \tag{1}$$

$$I_0(a_i) = \frac{1}{\pi}\int_0^{\pi} e^{a_i * cos\theta} d\theta \tag{2}$$

where a_i is the concentration parameter defining the dispersion of the ith fiber family, μ_i is the mean orientation angle of the ith fiber family. Finally, $I_0(a_i)$ is a zero order Bessel functions of type I, which acts as a normalization parameter such that:

$$\int_0^{\pi} f(\theta\|\mu_i, a_i) d\theta = 1 \tag{3}$$

If a is zero, the distribution tends to be uniform, whereas for very high values of a the distribution assumes a dirac-delta function about the mean orientation μ. Von-mises distribution is π-periodic such that $f(\theta) = f(\theta+\pi)$. By varying the mean and concentration parameters, the above function can represent a wide range of collagen organizations. In case of two fiber families, a mixture Von-Mises function is used: $f(\theta\|\mu_1, \mu_2, a_1, a_2, p) = p\frac{e^{a_1 cos2(\theta-\mu_1)}}{\pi I_0(a_1)} + (1-p)\frac{e^{a_2 cos2(\theta-\mu_2)}}{\pi I_0(a_2)}$. Here, $0 < p < 1$ is a parameter to determine the weight of each fiber family.

The orientation distribution is quantified by a single parameter called the orientation index (OI), which provides a measure of fiber alignment (Pasta et al., 2016) as shown in Eq. (4).

$$OI = \frac{1}{n}\sum cos^2(\theta_i) \tag{4}$$

where θ_i is the orientation of a fiber with respect to circumferential direction, n is the total number of fibers. A value of 1 for orientation index indicates that the fibers are perfectly aligned towards a preferred direction, where as a value of 0.5 indicates an isotropic alignment.

Collagen fiber waviness defines the initial crimp in the model and is related to the stretch at which collagen is recruited under loading. For this reason, all the images of the stack were analyzed semi-automatically to obtain fiber characteristics such as end-to-end length (l_s), and crimped length (l_c). These parameters were measured using ImageJ tracing and measuring tools, which was also demonstrated by Rezakhaniha et al. (2012) using NeuronJ, an ImageJ plugin for neurite tracing and analysis. The recruitment stretch of a collagen fiber is then defined by Eq. (5).

$$\lambda_r = \frac{l_c}{l_s} \tag{5}$$

As the above equation suggests, λ_r has a lower bound of 1. A value of 1 indicates that the fiber is straight in unloaded state. A value of $\lambda_r > 1$ indicates the amount of stretch in the fiber direction needed to engage the fiber in load bearing. The true stretch in the fiber can then be computed as $\lambda_{fiber} = \lambda/\lambda_r$. λ is defined as $l_{deformed}/l_s$. The value of λ_r increases with an increase in initial fiber crimp. The content of collagen fibers in the tissue was estimated using a fast marching segmentation technique. It requires the user to provide multiple seed points from which the contour expands along the fiber. Collagen volume fraction was then defined as the ratio of segmented voxels (VS) to total number of voxels (VT) prior to initiating segmentation.

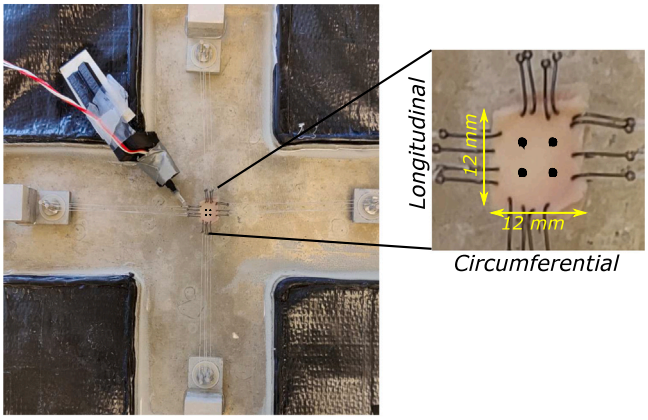

Fig. 2. Biaxial tension test setup showing the sample mounted with barbless hooks and sutures.

2.4. Mechanical testing

Samples were prepared as explained in Section 2.1 for mechanical testing. The samples were cut into a square shape of length approximately 10 − 12 mm. A graphene based dye was used to place four markers on the tissue around the center. This was done in order to follow the deformation of the sample via a high resolution, high speed camera (NIKON) set up for digital image correlation (DIC); whose frequency was set in the range of 2–5 Hz (Fagerholt et al., 2013). The sample was mounted on to the testing setup using four barbless hooks (Ahrex, Denmark) and surgical gore-tex sutures (Gore Medicals, USA) at each side as depicted in Fig. 2, while being submerged in PBS for the entire duration. The temperature of the PBS bath was maintained at 36.9 °C to mimic in-vivo conditions. The custom-built biaxial machine is equipped with four step motors that are individually controlled via an inductive displacement sensor (BAW M18MG, Balluff, Germany). The loads are also measured with an axial load transducer (U9C/50 HBM, Germany). Prior to performing the actual test, the sample was loaded with 3–5 preconditioning cycles up to 30% of strain in each loading direction. Once a satisfied result is achieved for preconditioning, the samples were deformed at a stretch rate of 0.2 min^{-1}. The biaxial machine was validated using a rubber-like material and compared to a commercial uniaxial machine (Instron, USA) (Sadeghinia et al., 2022). For each sample, three different configurations were tested: one with $\lambda_c : \lambda_l = 1$ (equibiaxial), one with $\lambda_c : \lambda_l > 1$, and one with $\lambda_c : \lambda_l < 1$. Here λ_c and λ_l represent the applied stretch in circumferential and longitudinal directions respectively.

2.5. Constitutive model for tracheal layers

Based on the investigations from MPM imaging and biaxial mechanical testing, structural constitutive models are proposed for the layers of the trachea, in order to incorporate fiber morphology information. Even though the affine nature of fiber kinematics has been extensively investigated and contested (Morin et al., 2018; Chandran and Barocas, 2006; Jayyosi et al., 2017), the model used in this study assumes affine transformation for fiber kinematics.

Continuum mechanics framework: The stretch of the material λ in any given direction represented by a unit vector e is defined as the ratio between its length in the deformed configuration and in the reference one, expressed as: $\lambda^2 = e : C : e$. Here, $C = F^T F$ is the right Cauchy–Green tensor, and $F = \partial x/\partial X$ represents the deformation gradient tensor. In order to easily handle the restriction of the quasi-incompressibility, a decomposition of $F = J^{1/3}F^{-}$ into volume-changing (dilatational) and volume-preserving (distortional) parts is generally established; where J is the local volume ratio, also called the Jacobian of the deformation (for a volume-preserving deformation J = 1).

Structural model: In order to characterize the anisotropic, quasi-incompressible mechanical behavior of the tissue layers, it is assumed that the strain energy density can be represented as a superposition of an isotropic potential (ψ_{iso}) for the ground matrix and an anisotropic potential for each fiber family (ψ_{fi}). The strain energy function can be written in the decoupled form for anisotropic materials as follows: $\psi = \psi_{iso} + \sum_{i=1,2} \psi_{fi}$. The strain–energy function proposed by Holzapfel et al. (2015) for fibrous materials, which could be adapted to one or two families of fibers, is used to predict the mechanical behavior of the tissue. The model assumes a planar distribution of fibers in the tissue, and will be referred to subsequently as 2-D GOH model (Gasser et al., 2006). Briefly, the isotropic part of the strain energy function is defined as,

$$\psi_{iso} = \frac{c}{2}(I_1 - 3) \quad ; \quad I_1 = trace(C) \tag{6}$$

where $c > 0$ is a material parameter and I_1 is the first invariant of C. Similarly, the anisotropic contribution of the ith fiber family is defined as,

$$\psi_{fi} = \frac{k_1}{2k_2}[e^{k_2 E_i^2} - 1] \tag{7}$$

where k_1 and k_2 are material constants and E_i are invariants based on the material structural tensor defined as,

$$E_i = tr(CH_i) - 1 \quad ; \quad H_i = \gamma_i I + (1 - 2\gamma_i)(M_i \otimes M_i) \tag{8}$$

where I is the 2nd order identity tensor, M_i is a unit vector in the direction of mean orientation of the ith fiber family, and γ_i is the dispersion parameter of ith fiber family; which is related to the Von-Mises concentration parameter through the equation: $\gamma_i = 0.5 - \frac{I_1(a_i)}{2I_0(a_i)}$, where a_i is the concentration parameter defining the dispersion of the ith fiber family, I_0 and I_1 are modified Bessel functions of first kind and order 0 and 1 respectively.

Given the planar biaxial loading, we denote the subscripts c, l to represent the two in-plane orthogonal directions: circumferential and longitudinal respectively. The out of plane axis is represented by the subscript z. The stretch components λ_c and λ_l are computed from the DIC measurements. Imposing the incompressibility constraint gives us $\lambda_z = \frac{1}{\lambda_c \lambda_l}$. Now, the deformation gradient tensor and right Cauchy–Green tensor can be written as:

$$F = diag[\lambda_c, \lambda_l, \lambda_z] \quad ; \quad C = diag[\lambda_c^2, \lambda_l^2, \lambda_z^2] \tag{9}$$

The mean fiber orientation unit vector can be written as $M_i = cos(\mu_i)e_c + sin(\mu_i)e_l$, where e_c and e_l are unit vectors along circumferential and longitudinal directions respectively. We define $h_i = FH_iF^T$ such that $tr(h_i) = tr(CH_i)$, whose diagonal components are defined in Eq. (10).

$$\begin{aligned} h^i_{11} &= [\gamma_i + (1 - 2\gamma_i)cos^2(\mu_i)]\lambda_c^2; \\ h^i_{22} &= [\gamma_i + (1 - 2\gamma_i)sin^2(\mu_i)]\lambda_l^2; \\ h^i_{33} &= 0 \end{aligned} \tag{10}$$

Finally, the isotropic and anisotropic components (corresponding to a fiber family) of the Cauchy stress tensor can be written as:

$$\begin{aligned} \sigma_{iso_c} &= c[\lambda_c^2 - \lambda_z^2] \\ \sigma_{iso_l} &= c[\lambda_l^2 - \lambda_z^2] \\ \sigma^i_c &= 2k_1(tr(CH_i) - 1)exp[k_2(tr(CH_i) - 1)^2]h^i_{11}; \\ \sigma^i_l &= 2k_1(tr(CH_i) - 1)exp[k_2(tr(CH_i) - 1)^2]h^i_{22}; \\ \sigma^i_z &= 0 \end{aligned} \tag{11}$$

$$\begin{aligned} \sigma^{total}_c &= \sigma_{iso_c} + \sigma^1_c + \sigma^2_c; \\ \sigma^{total}_l &= \sigma_{iso_l} + \sigma^1_l + \sigma^2_l; \end{aligned} \tag{12}$$

where c and l represent the circumferential, longitudinal components respectively. The superscript i in Eq. (8) through 10 is used to represent the number of the fiber family. It is to be noted that the stress components in Eq. (11) are derived by enforcing an incompressibility constraint, meaning the isotropic component is not a direct derivative of Eq. (5). It is to be noted that the isotropic material parameter is presumed to account for the contributions of ground matrix, elastin and smooth muscle (in the case of trachealis muscle). Based on MPM investigations, a two-fiber family was chosen for the adventitia, whose stress components are described by Eq. (11). In the case of mucosa and trachealis muscle a single fiber family was used to model the mechanical response. Given the structure and approximately linear mechanical response of the cartilage, a simple Neo-Hookean strain energy function was chosen to model it, which is defined in Eq. (6).

2.6. Inverse parameter identification

Quantified fiber morphology derived from MPM image stacks reduced the number of parameters to be identified. A cost function representative of standard error of estimate (SEOE) was built in Matlab® defined in Eq. (13) (Peddada and Haseman, 2005), based on the experimental and analytical stress–stretch responses. This function was subjected to a constrained optimization loop using genetic algorithm, a part of the optimization toolbox in Matlab®. Constraints were imposed on the parameters in order to ensure a uniform sampling of the initial population. Multiple runs of the optimization loop ensured that the identified parameter set does not correspond to local minima. The identified parameter set while minimizing the cost function value was accepted as the optimal value.

$$f = \sqrt{\frac{\sum_{i=1}^{n}(\sigma_{exp}(i) - \sigma_{Analytical}(i))^2}{n}} \tag{13}$$

In the above equation, n is the number of data points considered for each sample, following a spatial discretization of stretch ($n > 20$). σ_{exp} and $\sigma_{analytical}$ are the experimental and analytical stress values at each point on the discretized stretch domain. Optimal parameter set was identified for each sample which are presented in Tables 5, 6 and 7.

3. Results

3.1. Multi-photon microscopy

Fibrous networks of the tracheal microstructure revealed varying morphologies depending on the considered layer. Herein, MPM image stacks of adventitia, mucosa, and the trachealis muscle from one sample of each specimen are depicted here. The microstructure of the cartilage is discussed in Section 4. The fiber morphology of all samples from individual tracheal specimens is presented in Appendix A.

3.1.1. Adventitia

Collagen in the adventitia was observed to be organized in thick bundles, which were crimped in the load-free state. This is seen in the column 1 of Fig. 3, which represents a 2-d projection of an image stack from each specimen. The evolution of planar orientation of the fibers through the tissue's thickness is shown in Fig. 3 column 2, depicting the normalized intensity of fibers. With the color-bar, a relative amplitude of 1 indicates high fiber concentration in that direction, where as a relative amplitude of 0 indicates absence of fibers in that direction. It was evident from the analysis that the fiber morphology varied significantly from specimen to specimen. For instance, in the sample from specimen 3 the mean fiber orientation was characterized with two fiber families oscillating around the circumferential direction, with mean orientations of −8.7° and 23.4°. In contrast, the sample from specimen 4 showed two fiber families with mean orientations of −57.2° and 50.4°, aligning more towards the longitudinal direction. Remarkably, certain regions in the thickness exhibited more than two fiber families which could be seen in the 3rd column of Fig. 3 for instance in specimen 1 at 40%–50% thickness and in specimen 2 at 60%–80% thickness. The recruitment stretch as defined in Eq. (5) of the fibers in the load free state was computed to be 1.13±0.051. The layer displayed some material heterogeneity also in terms of collagen content, with an overall average volume fraction of 38.08 ± 2.06%. The quantified morphology for each specimen corresponding to the samples presented in Fig. 3 is reported in Table 2.

Table 2
Computed fiber morphology parameters of the Adventitia for all tested samples; sample 1 in each specimen corresponds to samples shown in Fig. 3.

Specimen	Sample	μ_1	μ_2	a_1	a_2	p	λ_r	VF
1	1	33.7	−29.4	2.27	1.12	0.60	1.14	37.41
	2	–	−8.72	–	0.42	–	1.19	36.73
	3	13.6	−88.7	0.27	0.75	0.54	1.11	41.11
2	1	36.5	−44.2	0.72	2.44	0.64	1.13	36.68
	2	37.3	−41.6	0.85	1.24	0.51	1.19	39.90
	3	40.6	−9.3	1.42	1.71	0.67	1.11	38.28
3	1	23.4	−8.7	0.61	1.91	0.65	1.16	40.58
	2	–	−6.3	–	1.12	–	1.08	34.71
	3	46.4	−46.7	1.06	0.97	0.48	1.10	36.56
4	1	50.4	−57.2	1.45	0.93	0.48	1.12	39.17
	2	41.4	−42.2	1.31	1.17	0.49	1.11	34.62
	3	42.1	−42.5	1.21	1.36	0.51	1.18	38.41
5	1	40.5	−44.7	7.12	6.64	0.41	1.12	38.27
	2	41.2	−44.5	1.82	2.04	0.53	1.07	40.18
	3	43.3	−61.4	0.52	0.29	0.43	1.09	38.64
	avg	37.7	−38.4	1.58	1.62	0.53	1.13	38.08
	std	9.7	22.9	1.74	1.51	0.08	0.05	2.06

3.1.2. Mucosa

The distinction between submucosa and mucosa is not possible to make with the naked eye. Hence, following the literature that much of the fibrous connective tissue is present in the submucosa layer (Downey and Samra, 2020), samples were sectioned away from the lumen. Collagen in this layer was also organized into thick bundles. However, unlike the fibers in the adventitia they did not agglomerate into several oriented bundles. Instead, in majority of cases a single fiber family was observed throughout the thickness. The 2-d projection of SHG image stacks, variation of orientation intensity along the thickness, and identified mean orientation of each fiber family for all specimens is depicted in Fig. 4. The variation of fiber orientation along the thickness was found to be insignificant compared to the adventitia. Although two fiber families were identified for a few thickness ranges, they amount to less than 20% of the overall contribution. The preferred mean orientation of the fibers varied between 17.5° in the sample from specimen 2 to almost diagonal organization in the sample from specimen 3 (44.6°). The dispersion of fibers was also observed to be slightly lower compared to the adventitia. The fibers were found to be crimped with an average recruitment stretch of 1.11±0.06. The average measured collagen content in the layer was 27.43 ± 1.65% across all samples.

3.1.3. Trachealis muscle

Fiber morphology in the tracheal smooth muscle was distinct from the above two layers. Unlike the dense fiber bundles found in the adventitia and the mucosa layers, the fibers were sparsely organized in the tissue through the thickness. Secondly, in terms of their preferred orientation, the fibers were aligned close to the longitudinal direction (−90° or 90°). The fibers in this layer displayed the least crimp with an average measured recruitment stretch value of 1.07 ± 0.028. Although the structure formed loose bands of fibers, the overall volume fraction was still measured to be substantially higher with an average of 31.41 ± 2.23% across all samples. The quantified morphology parameters of

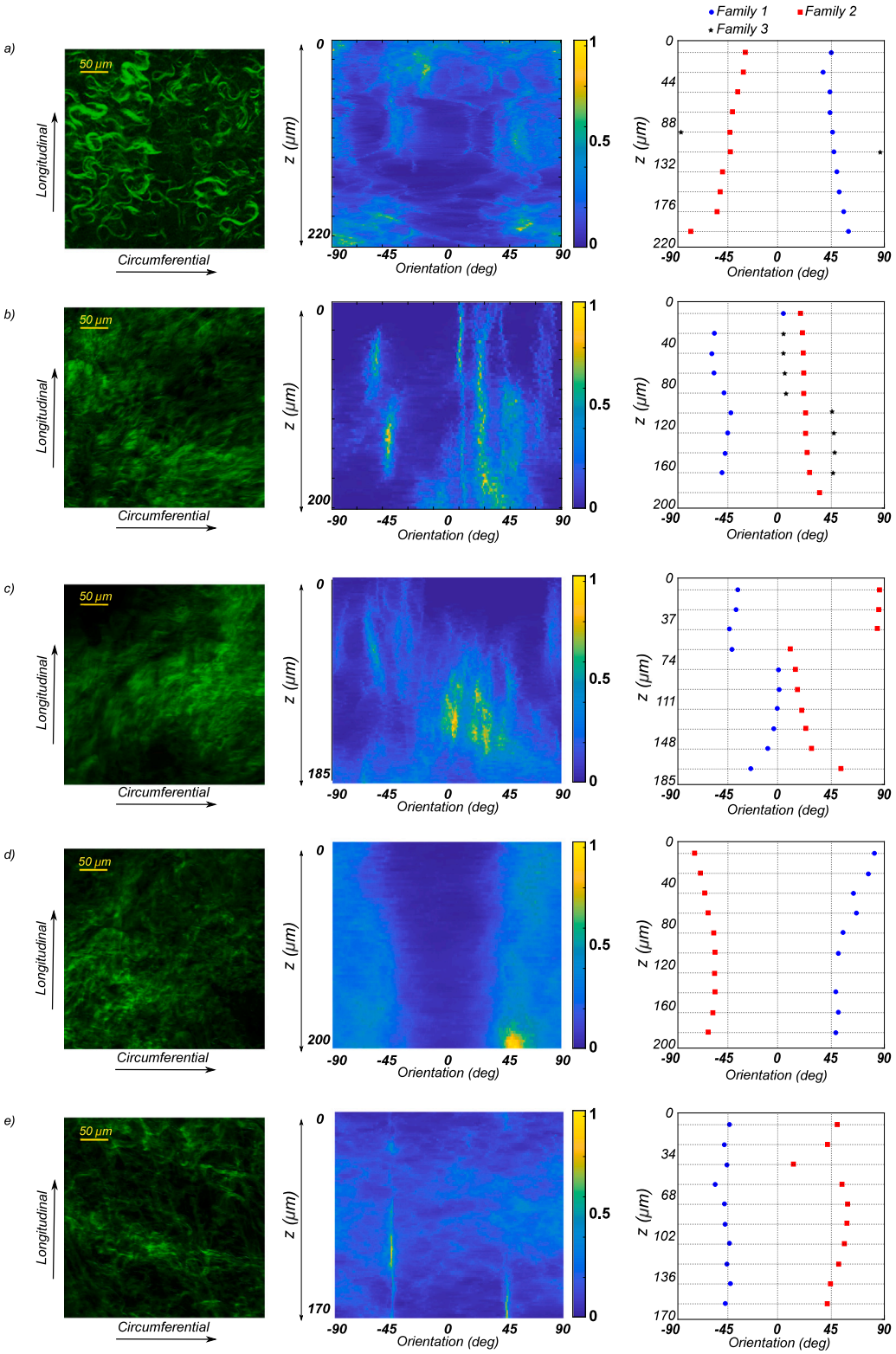

Fig. 3. SHG imaging of fibers in the adventitia. Column 1 (a–e) shows max-intensity projection of shg image stacks for a single sample from specimens 1 to 5; column 2 (a–e) shows the orientation intensity along the thickness of the tissue for each sample; column 3 shows an analysis of identified fiber families at various levels of the tissue's thickness for each sample. Orientation of 0 degrees corresponds to circumferential direction.

mucosa and the trachealis muscle for each specimen are presented in Table 3 (corresponding to samples depicted in Figs. 4 and 5). Intra-specimen variation of morphology in all samples is presented in Appendix A.

3.2. Mechanical behavior

The evaluated stress–stretch curves revealed a macroscopic anisotropy of the material's mechanical response. This is seen through

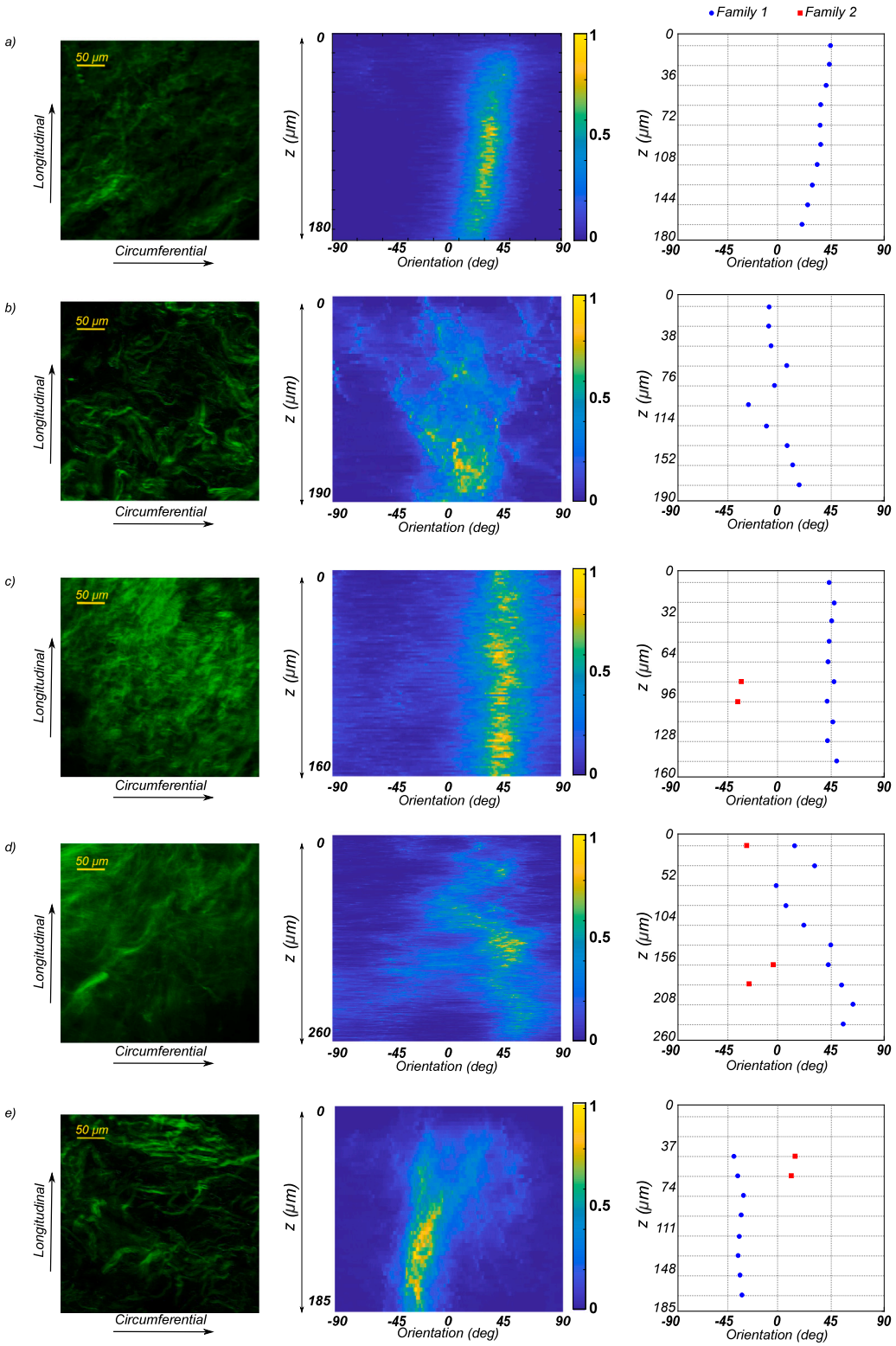

Fig. 4. SHG imaging of fibers in the mucosa. Column 1 (a–e) shows max-intensity projection of shg image stacks for a sample from specimens 1 to 5; column 2 (a–e) shows the orientation intensity along the thickness of the tissue for each specimen's sample; column 3 shows an analysis of identified fiber families at various levels of the tissue's thickness for each specimen's samples. Orientation of 0 degrees corresponds to circumferential direction.

two phenomena: (i) estimated elastic modulus in the final loading regime, (ii) gradual stiffening behavior especially characteristic in adventitia, mucosa, and the trachealis muscle. This can be clearly seen in Fig. 6. Although there is no unique definition, the anisotropy in each tissue layer has been quantified by the metric proposed by Choudhury et al. (2009) as shown in Eq. (14). Where E_c and E_l are the elastic moduli in the circumferential and axial directions respectively, measured in the final loading regime to mainly account for the contribution of the fibers corresponding to the same strain level in each loading direction. The computed anisotropy index (AI) and orientation index

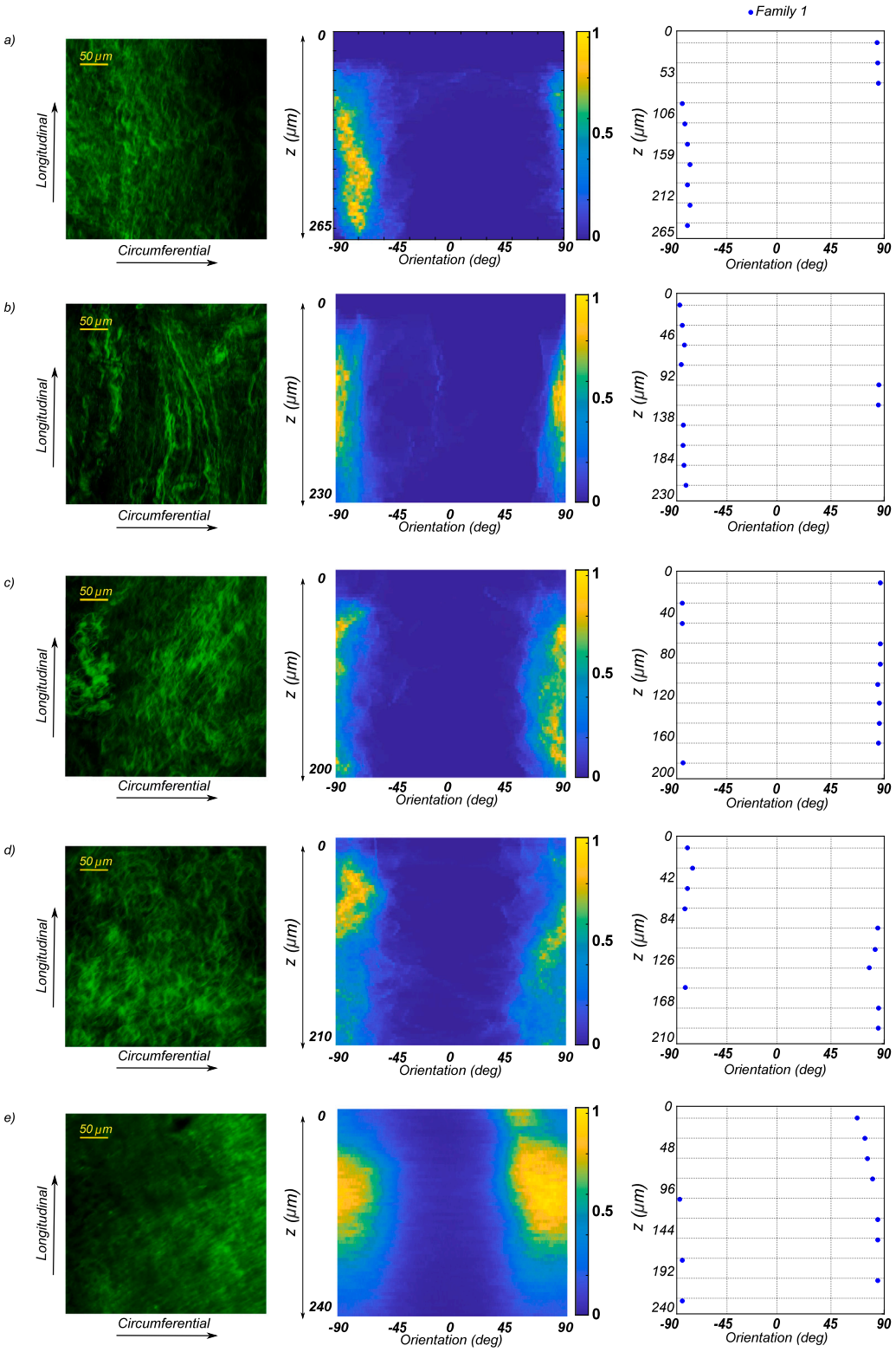

Fig. 5. SHG imaging of fibers in the trachealis muscle. Column 1 (a–e) shows max-intensity projection of shg image stacks for a sample from specimens 1 to 5; column 2 (a–e) shows the orientation intensity along the thickness of the tissue for each specimen's sample; column 3 shows an analysis of identified fiber families at various levels of the tissue's thickness for each specimen's sample. Orientation of 0 degrees corresponds to circumferential direction.

(OI) are presented in Table 4.

$$AI = 2 * \frac{E_c - E_l}{E_c + E_l} \tag{14}$$

Within the adventitia the elastic modulus displayed a sharp increase beyond 25% strain in the longitudinal direction and 35% in the circumferential direction as seen in Fig. 6, indicating the point at which

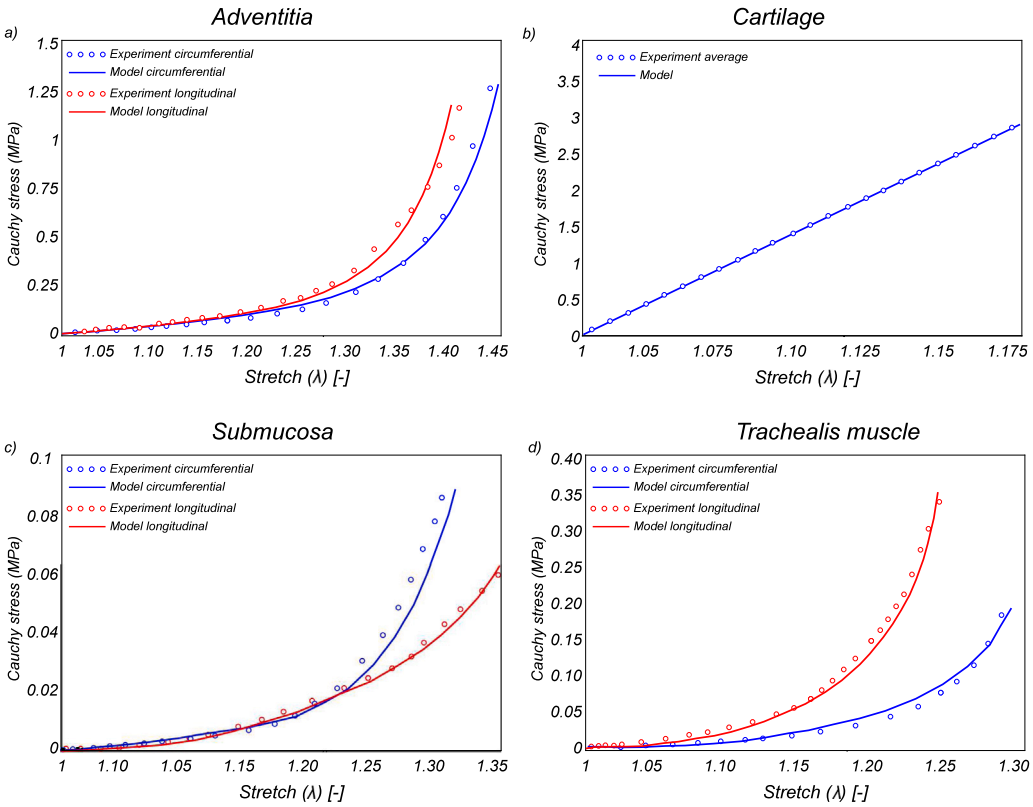

Fig. 6. Each subplot shows red and blue dotted lines representing experimental output of a single sample from specimen 1 in longitudinal and circumferential directions respectively and compared to constitutive model's output plotted with red and blue solid lines.

Table 3
Computed fiber morphology parameters of the Mucosa and Trachealis muscle for all samples tested; sample 1 in each specimen corresponds to samples shown in Figs. 4 and 5.

Specimen	Sample	Mucosa				Trachealis muscle			
		μ_1	a_1	λ_r	VF	μ_1	a_1	λ_r	VF
1	1	35.6	2.27	1.07	28.47	−79.4	2.68	1.06	32.68
	2	−37.4	1.31	1.16	26.51	77.1	0.76	1.12	29.42
	3	28.2	0.47	1.06	25.40	−74.5	3.42	1.06	34.74
2	1	17.5	0.72	1.15	27.11	88.1	1.57	1.09	31.19
	2	–	–	1.11	28.95	86.8	1.02	1.08	27.58
	3	−20.6	2.65	1.17	30.12	80.3	2.56	1.10	32.40
3	1	44.6	1.84	1.10	29.34	86.5	1.63	1.07	31.61
	2	−4.6	1.22	1.03	25.71	−82.7	1.68	1.05	33.14
	3	–	–	1.09	25.46	−76.4	1.36	1.05	28.06
4	1	42.1	1.07	1.14	27.45	−82.3	1.48	1.06	30.87
	2	−28.7	1.18	0.916	25.77	−86.2	2.07	1.03	29.15
	3	10.1	1.17	0.916	29.35	−84.3	2.11	1.03	30.47
5	1	−32.4	2.65	1.09	26.90	77.6	0.53	1.07	31.27
	2	28.5	0.37	1.08	26.54	−88.1	1.53	1.06	34.72
	3	45.2	0.81	1.06	29.65	−82.5	0.76	1.04	33.87
	avg	9.2	1.36	1.11	27.43	−86.8	1.67	1.07	31.41
	std	32.3	0.7	0.06	1.65	8.3	0.8	0.03	2.23

collagen fibers becomes the dominant load bearer. This observed difference in the recruitment of collagen fibers is attributed to the amount of reorientation and uncrimping they need to undergo in relation to each loading direction. The computed average anisotropy index of −0.18 at 37.5% strain indicated that the longitudinal direction is stiffer than the circumferential direction.

Unlike the other tissue layers, the cartilage displayed a relatively linear mechanical response. It is found to be the stiffest constituent of the wall. Overall, the elastic modulus was found to be greater in the circumferential direction (13.17 ± 2.64 MPa) than in the longitudinal direction (11.89 ± 2.18 MPa).

In contrast, the mucosa layer was found to have the least stiffness, with a maximum elastic modulus of 1.15 ± 0.12 MPa in the circumferential direction and 0.97 ± 0.08 MPa in the longitudinal direction. The average anisotropy index of 0.67 at 30% strain shows that the circumferential direction is stiffer than the longitudinal direction. Finally, the trachealis muscle exhibited a stiffer mechanical response in the longitudinal direction with a maximum elastic modulus of 4.77 ± 0.78 MPa as compared to 2.65 ± 0.57 MPa in the circumferential direction. This was also consistent with the average anisotropy index of −0.39 at 22.5% strain. The stiffening behavior was clearly less pronounced in the circumferential direction, which is dominated by smooth muscle fibers (Doeing and Solway, 2013), yet displayed a noticeable degree of non-linearity.

3.3. Structure based material model

In order to demonstrate the predictive capability of the proposed model, the analytical results obtained from the model were compared to experimental data. The structural data obtained from SHG images presented in Tables 2 and 3 were used as input in the constitutive model, i.e, the parameters to be identified from mechanical tests were C, k_1, and k_2. For the adventitia, a two fiber family model was found to be best suited in line with the observations made from SHG imaging. For samples showing more than 2 peaks in the FFT, peaks in close proximity were assumed to belong to a single fiber family in the identification process. The model showed a minimum r-squared value of 0.93. The cartilage was modeled with a neo-Hookean model which showed an excellent description of its mechanical response, with an average r-squared value of 0.99. The mucosa layer was modeled with a single fiber family even though a few samples showed multiple fiber families present in the thickness. The model predicted the tissue's

Table 4
The estimated anisotropy index and orientation index in each sample. Anisotropy index was computed at a strain of 0.375 in adventitia samples, at 0.30 in mucosa samples, and 0.225 in trachealis muscle samples.

Specimen	Sample	Adventitia		Mucosa		Trachealis muscle	
		A.I	O.I	A.I	O.I	A.I	O.I
	1	0.26	0.75	0.79	0.67	−0.26	0.058
1	1	0.31	0.92	0.54	0.63	−0.25	0.063
	1	−0.37	0.88	0.49	0.71	−0.14	0.071
	1	−0.27	0.74	0.73	0.85	−0.82	0.003
2	1	−0.31	0.73	−0.15	0.53	−0.45	0.027
	1	−0.23	0.79	0.62	0.83	−0.29	0.051
	1	0.21	0.84	0.21	0.40	−0.45	0.024
3	1	0.37	0.95	0.84	0.95	−0.36	0.032
	1	−0.54	0.67	0.35	0.57	−0.21	0.066
	1	−0.79	0.44	0.31	0.60	−0.35	0.035
4	1	−0.44	0.72	0.72	0.75	−0.52	0.009
	1	−0.29	0.70	0.79	0.90	−0.42	0.031
	1	−0.52	0.65	0.17	0.55	−0.24	0.064
5	1	−0.23	0.58	0.81	0.72	−0.66	0.006
	1	0.21	0.57	0.31	0.43	−0.34	0.042
	avg	−0.18	0.74	0.67	0.70	−0.39	0.04
	std	0.35	0.14	0.15	0.21	0.16	0.02

Table 5
Fitted material parameters for all samples from the Adventitia and Cartilage.

Specimen	Sample	Adventitia					Cartilage		
		c (kPa)	k_1 (kPa)	k_2 (–)	SEOE	R^2	c (MPa)	SEOE	R^2
	1	8.4	62.1	1.4	0.28	0.95	3.6	1e−5	0.99
1	2	13.1	28.7	3.9	0.61	0.88	3.4	1e−5	0.99
	3	5.6	70.4	2.5	0.22	0.97	3.9	1e−5	0.99
	1	14.7	52.2	3.8	0.60	0.90	4.1	1e−5	0.99
2	2	20.6	71.9	1.2	0.33	0.95	3.8	1e−5	0.99
	3	11.8	38.5	2.7	0.30	0.96	3.6	1e−5	0.99
	1	10.4	64.4	2.6	0.55	0.88	3.7	1e−5	0.99
3	2	7.6	48.9	1.4	0.21	0.95	3.9	1e−5	0.99
	3	13.1	34.7	4.4	0.25	0.95	4.2	1e−5	0.99
	1	8.9	38.7	4.5	0.48	0.90	4.3	1e−5	0.99
4	2	11.7	53.1	5.7	0.23	0.96	4.2	1e−5	0.99
	3	6.1	21.7	12.2	0.27	0.96	3.6	1e−5	0.99
	1	12.4	37.3	3.1	0.36	0.92	3.8	1e−5	0.99
5	2	8.8	42.2	8.9	0.34	0.90	3.7	1e−5	0.99
	3	13.6	67.4	5.6	0.19	0.97	3.9	1e−5	0.99
	avg	11.4	48.8	4.3	0.37	0.93	3.8	1e−5	0.99
	std	3.8	15.8	2.9	0.15	0.04	0.2	–	–

Table 6
Fitted material parameters for all samples from the mucosa.

Specimen	Sample	Mucosa				
		c (kPa)	k_1 (kPa)	k_2 (–)	SEOE	R^2
	1	1.2	6.2	5.2	0.02	0.91
1	2	3.2	4.4	8.4	0.04	0.88
	3	0.7	2.7	4.5	0.02	0.93
	1	1.7	3.5	7.4	0.06	0.88
2	2	2.4	8.3	4.2	0.05	0.88
	3	0.8	11.2	5.1	0.05	0.87
	1	0.6	3.8	6.1	0.03	0.90
3	2	0.8	2.9	4.8	0.02	0.92
	3	1.2	1.8	7.2	0.02	0.91
	1	1.5	6.3	8.1	0.03	0.89
4	2	0.8	3.7	9.4	0.05	0.86
	3	0.5	1.9	6.4	0.02	0.93
	1	0.2	8.6	5.2	0.07	0.88
5	2	0.8	3.1	6.7	0.04	0.90
	3	0.5	11.7	4.8	0.02	0.95
	avg	1.2	5.4	6.2	0.036	0.89
	std	0.6	3.2	1.6	0.016	0.03

Table 7
Fitted material parameters for all samples from the trachealis muscle.

Specimen	Sample	Trachealis muscle				
		c (kPa)	k_1 (kPa)	k_2 (–)	SEOE	R^2
	1	9.3	10.3	16.8	0.17	0.90
1	2	12.7	7.4	12.7	0.13	0.93
	3	14.4	12.3	14.1	0.12	0.91
	1	12.5	6.7	11.8	0.21	0.89
2	2	18.2	5.2	13.5	0.17	0.91
	3	12.9	14.19	16.2	0.15	0.93
	1	10.4	12.4	9.1	0.11	0.94
3	2	22.1	6.6	7.8	0.10	0.92
	3	16.7	15.2	9.8	0.12	0.90
	1	13.2	6.8	10.5	0.11	0.91
4	2	11.8	4.7	14.2	0.11	0.94
	3	18.6	5.3	9.4	0.09	0.93
	1	14.7	14.1	13.3	0.12	0.90
5	2	12.9	18.4	10.8	0.07	0.92
	3	15.4	12.5	16.4	0.08	0.91
	avg	14.3	10.1	12.4	0.11	0.92
	std	3.4	4.2	2.8	0.03	0.02

mechanical response relatively well with a minimum r-squared value of 0.89. Finally, the trachealis muscle was also modeled with a single fiber family which provided a reasonable description of its mechanical response with a minimum r-squared value of 0.92. The goodness of fit for all the tracheal components can be seen in Fig. 6, the results correspond to sample 1. The identified material parameters for each tracheal component are presented in Tables 5, 6 & 7.

4. Discussion

4.1. Main contributions

To the best of our knowledge, this is the first experimental study investigating the morphology of fibers of different tracheal tissue layers, including adventitia, mucosa and trachealis muscle. Apart from the cartilage, all layers displayed a network of fibers, either loosely organized or in thick bundles, with an initial crimp. Adventitia was characterized by a highly dispersed distribution of fiber orientations, often represented by two fiber families. The mucosa layer displayed thick fiber bundles often organized into a single fiber family, aligned close to the circumferential direction. Within the adventitia and the mucosa, the fiber morphology showed a strong heterogeneity both with the sample and in between samples. Remodeling and re-organization of collagen can occur both under physiological and non-physiological loads (Cyron and Humphrey, 2017). The variation in collagen organization could be understood by the need to maintain homeostatic state in-vivo and influence the adaptive mechanical response. However, the exact explanation for this heterogeneity is poorly understood at the moment. The fiber morphology of the trachealis muscle was characterized by the presence of longitudinally aligned fibers with little dispersion. This information further led to structure based material modeling, with each fibrous layer identified with an anisotropic strain energy function.

4.2. Microstructure of cartilage

The matrix of hyaline cartilage contains primarily type II collagen, but types IX, X, and XI and other minor collagens are also present in small quantities. Type II collagen does not form large bundles, although the bundle thickness increases with distance from the lacunae (Gartner and Hiatt, 2006). The reason for excluding the morphology analysis of the tracheal cartilage is multi-fold. Firstly, the structure has been studied extensively with various imaging modalities (Jeffrey and Watt, 2003; Cova and Toffanin, 2002). Although the origin of the tissues used

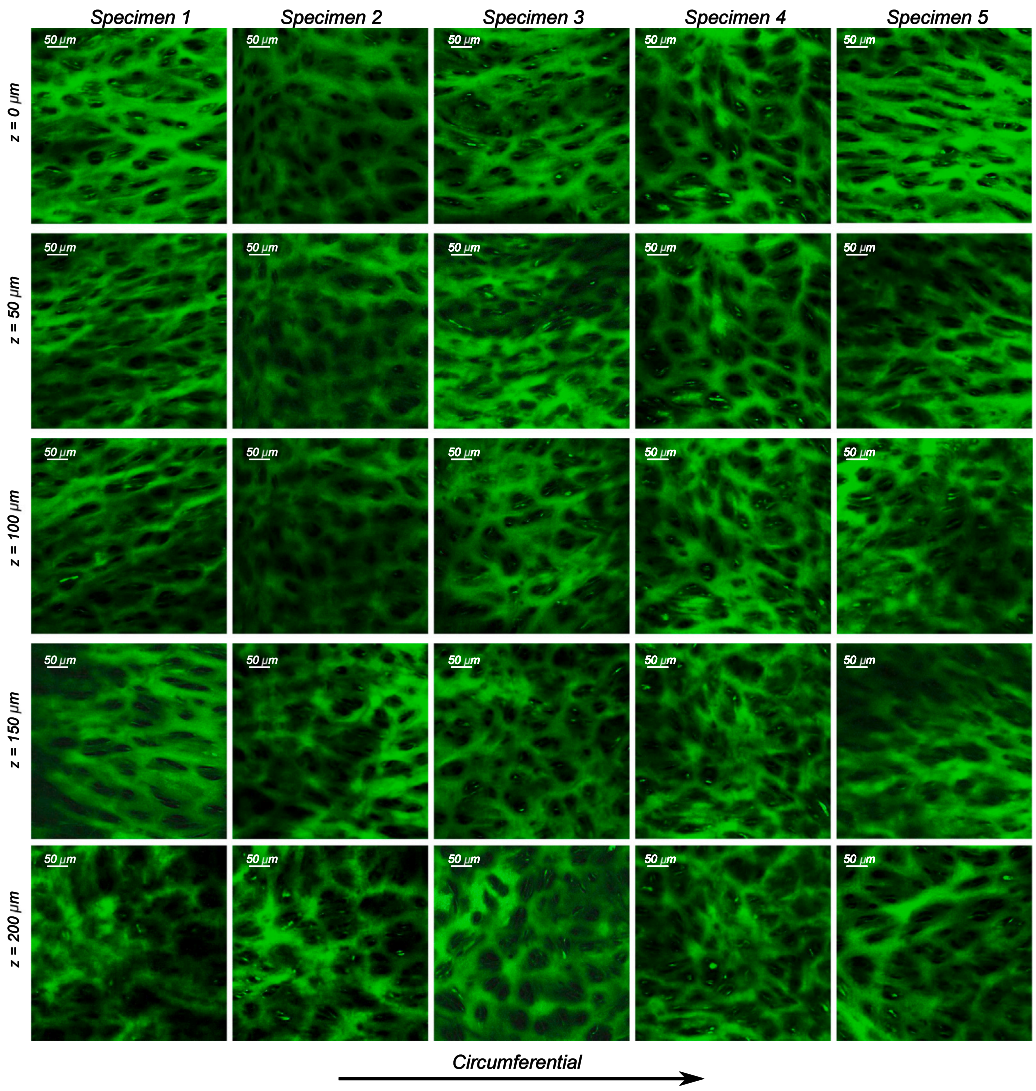

Fig. 7. SHG imaging of collagen-II in the tracheal cartilage at multiple levels in the thickness in each specimen.

in the above studies do not correspond to the trachea, the structure of hyaline cartilage is identical through out the body and thus provides an excellent understanding of the elaborate mesh-work of collagen type-II through out the cartilage. Secondly, the MPM images acquired on the tracheal cartilage displayed a consistent structure through the thickness as shown in Fig. 7, which is in line with previous reports (Zhu et al., 2016). Finally, the disparity in the morphology among different cartilage rings, and different specimens was seen to be insubstantial.

4.3. Longitudinal fibers of trachealis muscle

For a long time after the initial reports by Miller (1913), the tracheal muscle was presumed to be composed of circumferentially aligned smooth muscle fibers. The presence of longitudinal fibers in the tissue layer has been a topic of much debate. Although many reports indicate the presence of longitudinal fibers (Macleod and Heard, 1969), some reports (Hakansson and Toremalm, 1968) dispute that information. The results of our study from MPM image stacks of the tissue layer clearly indicate longitudinally aligned fibers. Secondly histological staining of the layer also showed mixed results, with some studies reporting the presence of two orthogonal families of collagen fibers (Trabelsi et al., 2010), and with other studies reporting longitudinal and oblique muscle fibers (Kamel et al., 2009). Our results are not consistent with the description of arrangement of fibers in the trachealis muscle suggested by Trabelsi et al. (2010). This is possibly because the author deduced collagen fiber morphology based solely on histology staining, which does not provide enough information for such a characterization. However, the excitation frequency for skeletal muscle and collagen is in the same range (Tiaho et al., 2007; Odin et al., 2008), thus imaging both molecules simultaneously in our protocol. The mechanical response could provide some insight on this discussion, given the softer response in the longitudinal direction compared to collagen rich adventitia. This could mean that muscle fibers dominate the structure as collagen fibers are much stiffer than muscle fibers (Herbert and Gandevia, 2019). This is substantiated by the reports that muscle fibers are often intertwined with collagen fibers inside the tissue (Kovanen et al., 1984), although their relative incidence has not been quantified.

4.4. Mechanics

Planar biaxial testing is a better representation of tissue's in-vivo deformation behavior as compared to uniaxial testing. This would in turn ensure the proper fiber kinematics influencing the tissue's mechanical response. To the best of our knowledge only one study has been reported to have conducted biaxial tension testing on tracheal tissue (Nemavhola et al., 2021). However, they do not test individual tissue layers, thus upholding the novelty of our test results. The tracheal cartilage was found to be the stiffest component with an

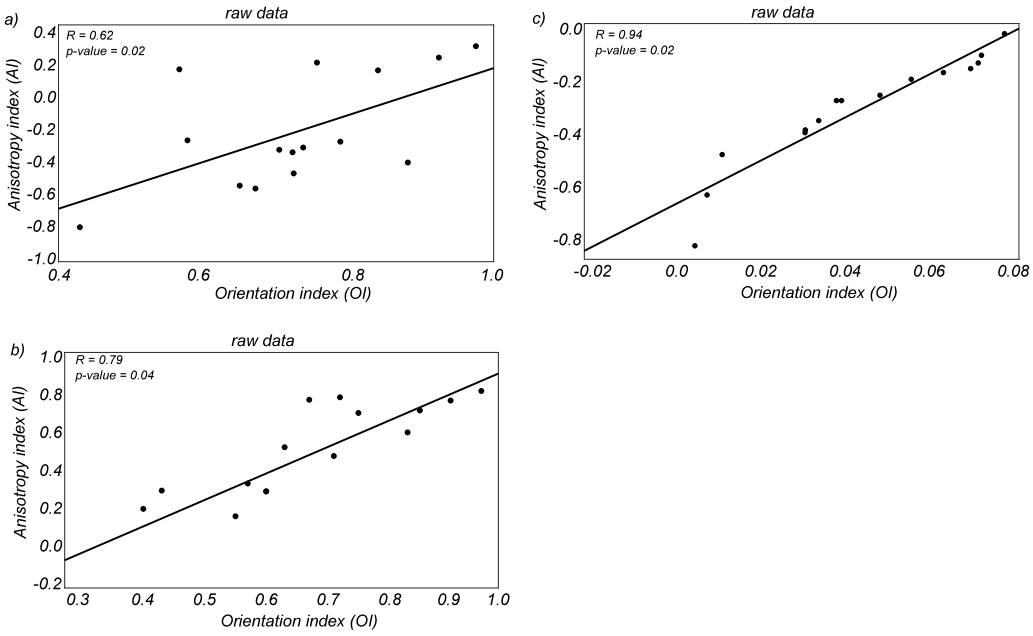

Fig. 8. Correlation between fiber morphology and mechanical response computed on all data points for: (a) adventitial layer, (b) mucosa/submucosa layer, (c) trachealis muscle layer.

average elastic modulus of 12.2 MPa. It was also seen that the cartilage practically exhibited a linear response within 20% strain, contrary to a few reported studies (Teng et al., 2008). However, the cartilage rings are interconnected with connective tissue, which might not reflect its true mechanical response in the biaxial test setup. For this purpose, individual cartilage rings were isolated ($n = 5$) and tested along the circumferential direction under uniaxial tension. The results showed a sharp increase in the identified elastic modulus, with an average value of 18.7 MPa. The other tissue layers including the adventitia, mucosa, and trachealis muscle exhibited a non-linear response, with significant stiffening beyond a certain load. Looking at the average mechanical response of each layer in isolation and collectively, the cartilage appears to act as the principal load bearing component. Similarly, it is suggestive that a portion of collagen fibers appear to engage in load bearing at 20% deformation. We believe that at extreme loading levels, as more collagen fibers engage in load bearing, they contribute to protecting the tissue from over-extension. On the other hand, the mechanical response of the trachealis muscle challenges its role in overall tracheal mechanics. It is traditionally believed that the main role of tracheal muscle is to facilitate the contraction of tracheal diameter via smooth muscle fibers. However, the stiffer longitudinal response and the presence of longitudinal muscle and collagen fibers suggests that it plays a role in limiting its displacement along the longitudinal direction.

4.5. Structure function relationships

The correlation of orientation index was computed with respect to anisotropy index described in Eq. (14) in order to understand structure function relationships. A strong correlation between O.I. and A.I. indicates the strong influence of structural organization of fibers on the tissue's macroscopic mechanical response. The trachealis muscle showed a strong correlation between the orientation and anisotropy indices for all samples with a minimum r-value of 0.94 and a p-value of 0.02 as seen in Fig. 8.e. In the case of trachealis muscle it was unexpected with the presence of smooth muscle fibers along the circumferential direction (not imaged in this study). On the other hand, a weaker correlation between O.I. and A.I. was observed in both the adventitia and mucosa layers, as shown in Fig. 8(a&e). The correlation coefficient was also computed within grouped data:

- Intra-specimen: Computed over all samples for each layer taken from the same specimen (3 data points per group).
- Inter-specimen: Computed over all samples for each layer excised from a similar location on the trachea (one per specimen, 5 data points per group).

Within all the layers, no statistical significance was observed for the intra-specimen group apart from specimen 2 in the mucosa. On the contrary, the inter-specimen correlation was found to be statistically significant in all the layers, apart from sample 1 in adventitia and sample 2 in mucosa. This could imply that the heterogeneity within samples excised from different locations of a given specimen is higher as compared to samples excised from different specimens but from identical anatomical location. All the grouped correlation plots are presented in Fig. 9. It should however be noted that data points in both analysis are too few to draw reliable conclusions. More data points from a single specimen excised from different locations along the circumference and along the length of the trachea would improve this understanding.

Secondly, the use of clearing agents like SeeDB (Ke and Imai, 2014) could significantly improve the scan depth which would in turn provide more micro structural information. While this was not performed in this study, it will be utilized in the ensuing investigations. Finally, the MPM image window was set at $465 \times 465\ \mu m^2$, centered around the four DIC markers, where as the size of the sample used to mechanical testing was $10 - 12$ mm. This could be overcome by either increasing the field of view or imaging several zones on the sample or a combination of both. However, it is either computationally expensive or heavily time consuming to do so.

4.6. Structure based material modeling

A thoroughly investigated and quantified fiber morphology reinforced the employment of structural constitutive models, which were developed for arterial tissue (Holzapfel et al., 2015). The adventitia/connective tissue has been modeled previously with Mooney–Rivlin and Yeoh hyperelastic models (Safshekan, 2016). These models were found to describe the adventitia's mechanical response from our tests accurately (r-square > 0.94). However, the 2-D GOH model takes into account additional structural information in terms of fiber dispersions,

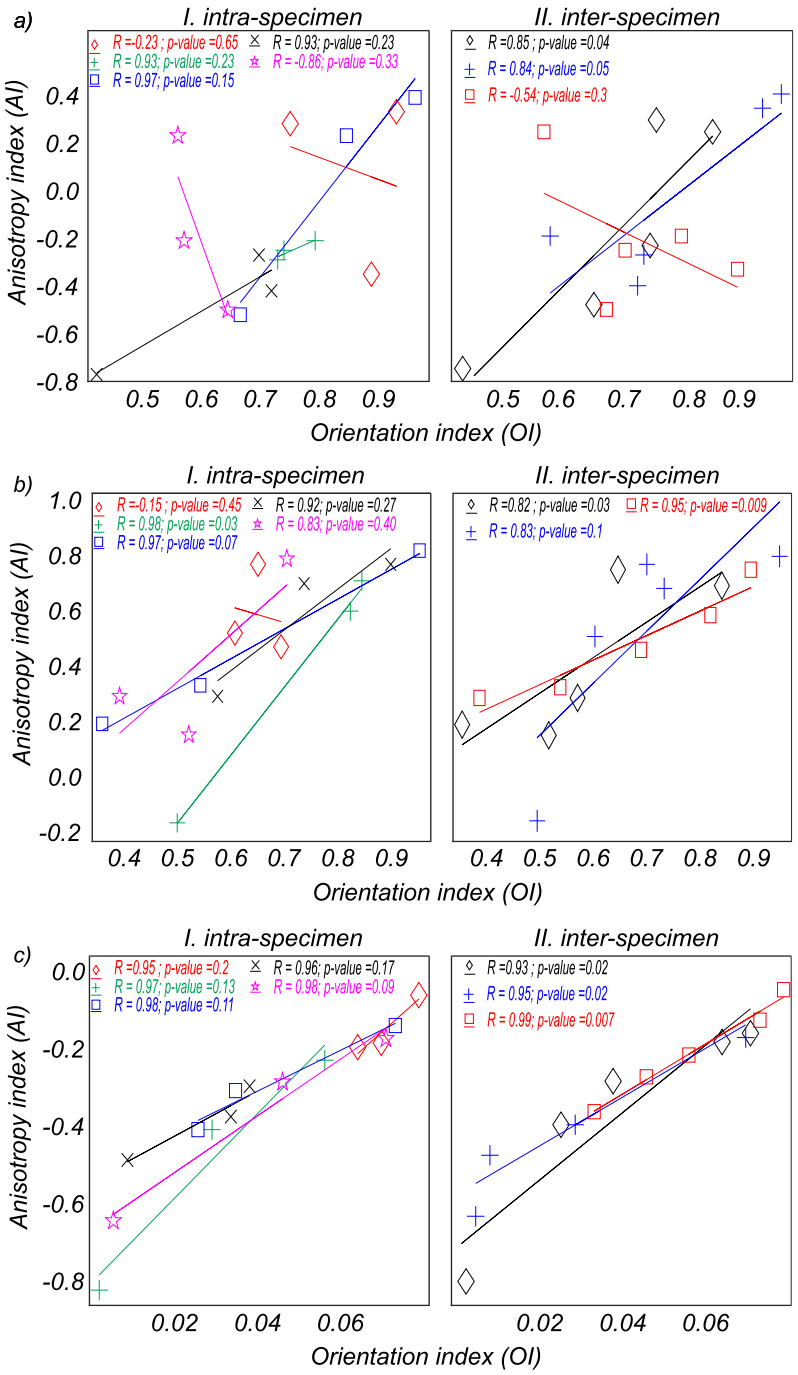

Fig. 9. Correlation between fiber morphology and mechanical response computed on grouped inter-specimen and intra-specimen data points for: (a) adventitial layer, (b) mucosa/submucosa layer, (c) trachealis muscle layer.

which is lacking in the above mentioned phenomenological models. In the case of cartilage, a Neo-Hookean model provided an excellent estimate of the mechanical behavior (r-square > 0.99) even though the test results showed a small degree of anisotropy. Aside from Neo-Hookean, the cartilage has also been modeled with Mooney–Rivlin and Yeoh hyperelastic models, with all of them offering an equally good fit to mechanical test data. The structure of the cartilage as seen from the MPM shows a tight mesh-work of collagen type-II in contrast to bundles of dispersed fibers found in the other layers. The anisotropy seen in the mechanical response could be arising from the collagen-II morphology, however given that it is quite low compared to other tissue components, it is reasonable to assume an average mechanical response. There is no data currently on the hyper-elasticity of the mucosa layer. Our investigations show that the 2-D GOH model with a single fiber family could provide an accurate description of its anisotropic mechanical behavior (r-square > 0.90). On the other hand, the trachealis muscle was identified with an anisotropic hyperelastic model (Holzapfel et al., 2005) as well as Yeoh and Mooney–Rivlin phenomenological models. However, the utilized structural model does not accommodate for fiber dispersions and only assumes two neatly aligned fibers (one circumferentially and one longitudinally). The model has since been updated to address this limitation, which is employed in this study to incorporate the quantified fiber morphology. It showed a good fit with an average r-square value of 0.92.

4.7. On pre-stress in the trachea

Residual stresses and strains are important in maintaining the homeostatic state. The zero-load state when the whole trachea is excised from the body does not correspond to its zero-stress state. Han and Fung (1991) measured the opening angles in dog and pig specimens, which represents the zero-stress state when the tissue is cut open along the longitudinal axis. In dogs, they reported opening angles of 180 degrees and 60 degrees when the tissue is cut open at the anterior (cartilaginous) and posterior (muscular) side respectively. Similar tests conducted on porcine tracheae showed significantly lower opening angles of 10 degrees with no significant regional differences. Rat tracheal specimens were used to measure the variation in opening angle along the longitudinal and circumferential directions (Liu et al., 2002; Teng et al., 2004). In concurrence with dog specimens, the opening angle was reported to be higher in the anterior end compared to the posterior side. While the opening angles were identical along the longitudinal direction at the posterior side, they were reported to increase at the anterior side. These reports clearly demonstrate that residual stresses in the trachea are non-uniformly distributed. Even though the structure based constitutive model reported here allows for the computation of stress-state in the tissue, it is incomplete without the knowledge of zero-stress state of the trachea. For further development, residual stress measurement should be taken into account to improve the modeling process, which were not measured in this study.

4.8. Comparison between bovine and human trachea

Microstructure: The fibrous connective tissue of the human airways is composed of a dense network of collagen and elastin fibers embedded in a ground matrix (Young et al., 1980). The structure was found to be similar in our investigations of bovine tracheal connective tissue, which displayed random distributions of dense collagen fiber bundles. The hyaline cartilage, which is primarily made up of collagen-II also showed a similar native structure in both human 2-photon imaging and bovine MPM imaging, with both showing a meshwork of extracellular matrix and lucanae. Although, the microstructure of mucosa in human trachea has not been studied for an objective comparison, histology staining of porcine tissue revealed networks of collagen and elastin fibers embedded in the tissue close to the lumen surface (Eskandari et al., 2019). There also seems to exist a layer of fibrous connective tissue deep into the tissue (>1000 μm), which could not be imaged in this study. As suggested in Section 4.3 the presence of longitudinal fibers in the trachealis muscle has been contested. Histology staining of human tissue revealed two orthogonal families of fibers (Trabelsi et al., 2010), which has not been observed in our investigation of the tissue.
Mechanics: Mechanical testing of the adventitial layer in humans revealed the circumferential direction to be stiffer than the longitudinal direction (Teng et al., 2012), with a strong stiffening response. The results from Safshekan (2016) however show a more gradual stiffening response. Our results from bovine tissue do show that the circumferential direction is stiffer, however less pronounced. Given the highly varying microstructure of the layer, the uncertainty in its mechanical response can be complicated to quantify. Human cartilage has been extensively tested via uniaxial tension tests. Assuming linear elasticity, the average Young's modulus has been reported to be 3.3 MPa in Trabelsi et al. (2010), 12 to 15 MPa in Rains et al. (1992), and 8 to 24 MPa in Safshekan (2016). Although there seem to be a significant variation in tracheal cartilage stiffness in humans depending on age, the Young's modulus of bovine trachea (13.57 MPa) is in agreement with that of an average adult human tissue. The sole data for mechanical behavior of the mucosa layer is reported in Teng et al. (2012). Direct comparisons to the data presented there show that the circumferential direction is stiffer in both human and bovine tissue. However, a strong stiffening behavior is observed in human tissue, which was not observed in bovine tissue. For instance, the measured pseudo elastic modulus as 20% strain in human tissue was 76.8 MPa where as in bovine tissue the maximum measured value was 1.6 MPa. A similar trend was observed in the trachealis muscle, with two of the three tested samples showing strong stiffening in the longitudinal direction. This was absent in our investigations, with the maximum measured modulus of about 6 MPa in the longitudinal direction as compared to reported value of 34 MPa in humans at the same stretch. The study conducted by Safshekan (2016) reports a modulus of 4.1 MPa which is more in agreement with the value observed in our investigations. However, the directional dependence of the result is not mentioned in the study, even though it considers a much larger sample set of 30 as compared to 3 in Teng et al. (2012).

4.9. Limitations

Despite the many interesting findings reported in this study, limitations exist:

1. As important as collagen is, it is not the only structural constituent lining the tracheal wall. The other structural constituents such as elastin and smooth muscle cells play an important role in the passive and active mechanical response of the tissue respectively. This is particularly important in the trachealis muscle as it is well established that smooth muscle cells align circumferentially in the layer. Elastin fibers are present in the mucosa layer as well as the adventitia. Their structural organization could provide more insights into tracheal mechanics, but is not considered in this study.
2. The length of the trachea is around 12 cm s in an average human. Given the inherent heterogeneity and anisotropy of the material, the current study is limited on location dependent analysis of the microstructure morphology
3. A similar comment could be made on the examined area and depth. The tissue layers lining up the trachea are up to 2–3 mm in thickness. The imaged stack volume does not encompass the whole tissue.
4. We analyzed the planar collagen fiber orientation using only the 2D data, assuming that the fibers are mainly lying in the circumferential–longitudinal plane. This choice was motivated by previous histology studies (Eskandari et al., 2018), but in the future out-of-plane contribution should be examined.
5. Along the with microstructure, the role of smooth muscle fibers mechanics has been neglected here. Only the passive mechanical behavior was characterized, which prompts questions on the role of trachealis muscle in overall tracheal mechanics.
6. The constitutive model used to describe the mechanical response of the tissue assumes affine transformation, which could lead to an over-estimation of material parameters.

5. Conclusion

Through this study, we have shown that tracheal microstructure presents significant inter-layer differences in collagen fiber network morphologies. These inter-layer differences concern in particular the ability of the fibers to re-organize themselves under in-vivo loading, giving each of them a different role in the load-bearing. These finding brings additional insight for current structural material model formulations, which take into account specific kinematics of collagen and its relation to the surrounding matrix. It also affirms the need to consider the trachea as a multi-component structure, composed of different mechanically significant layers. Furthermore, we have shown that there exist significant heterogeneity in collagen fiber network morphology within a given layer, except the cartilage. In addition to random organization of the fibers in each layer, they were also crimped when observed in an unloaded state. On the other hand, biaxial testing of the tissue has suggested that anisotropy and non-linearity is prevalent

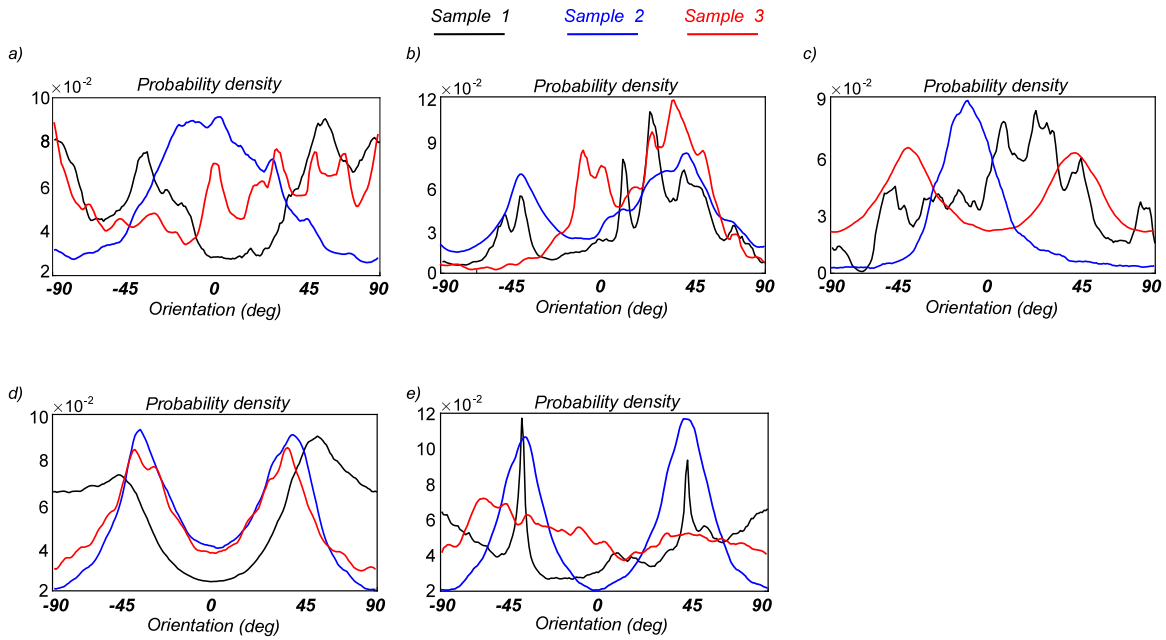

Fig. A.10. Intra specimen fiber morphology variation in Adventitia.

in all the layers. Both the phenomena could be explained easily with the random organization of fibers in conjunction with an initial crimp. It has been shown that the cartilage is the stiffest component of the tissue and most likely the principal load bearing component under healthy, physiological conditions. The relatively poor correlation of microstructure to tissue-scale mechanics in the adventitia and the mucosa layers suggest the need to further investigate the layers' structural composition. Nonetheless, these findings provide novel insights into the micro-architectural changes within the tracheal wall, with special regard to using it as a model for studies in human trachea.

CRediT authorship contribution statement

Venkat Ayyalasomayajula: Writing – review & editing, Writing – original draft, Validation, Methodology, Investigation, Formal analysis, Data curation, Conceptualization. **Bjørn Skallerud:** Writing – review & editing, Validation, Supervision, Software, Resources, Project administration, Methodology, Investigation, Funding acquisition, Conceptualization.

Declaration of competing interest

The authors declare that they have no known competing financial interests or personal relationships that could have appeared to influence the work reported in this paper.

Data availability

No data was used for the research described in the article.

Acknowledgments

We would like to thank Astrid Bjørkøy, PhD (Senior Engineer, Department of Physics, NTNU, Trondheim, Norway) for her assistance in sample preparation and discussion on acquiring SHG image stacks.

Appendix A. Intra-specimen variation

For each specimen, 3 samples were excised from three different locations along the trachea. Analysis of MPM image stacks from the samples marked the presence of inherent anisotropy of the material. Within the adventitial layer, the structural organization of fibers varied significantly from sample to sample. For instance in Fig. A.10 a, the orientation distribution varied from two diagonally (−45° or 45°) oriented families in sample 1 to circumferentially aligned single fiber family in sample 2 to an almost isotropic distribution in sample 3. Specimen 4 is seen as an exception as all samples displayed two fiber families with diagonal organization as depicted in Fig. A.10 d. The quantified orientation probability density for all samples is presented in Fig. A.10.

Fig. A.11 shows the orientation distribution of fibers corresponding to all samples of the mucosa layer. Although each specimen exhibited a huge variation in terms of fiber orientation, it could be ascertained that the preferential orientation was never observed to be close to the longitudinal direction (−90° or 90°). It varied from circumferential alignment (0°) to diagonal (−45° or 45°), with 3 of the 15 samples exhibiting two fiber families.

The trachealis muscle samples showed the least diversity in fiber morphology as seen in Fig. A.12. All samples exhibited a preferred fiber orientation close to longitudinal direction (−90° or 90°) regardless of the specimen. In some cases, specially pronounced in specimen 1 and 5, some obliquely oriented fibers were present (shown in Fig. A.12 a and e). Overall, this layer also exhibited the least amount of fiber dispersion.

Appendix B. Whole tissue vs composite layup

The whole tracheal tissue was tested without separating the components attached to the cartilage for one specimen. For individual layers, the force required to stretch the tissue in the circumferential direction to the same level as in the whole tissue is recorded. The composite stress

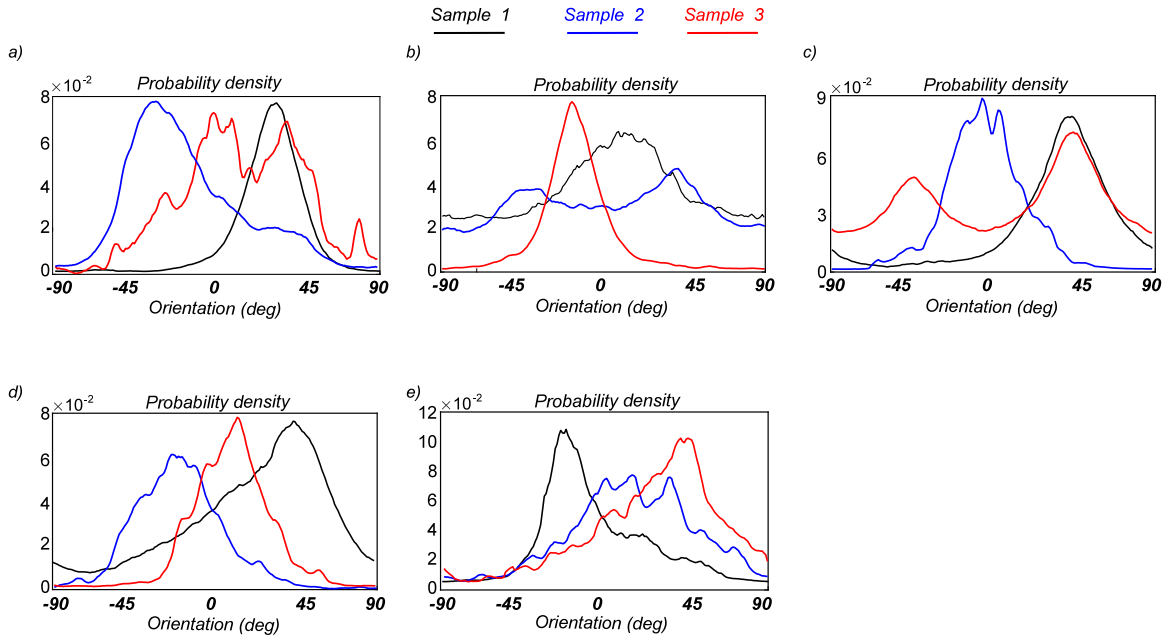

Fig. A.11. Intra specimen fiber morphology variation in Mucosa.

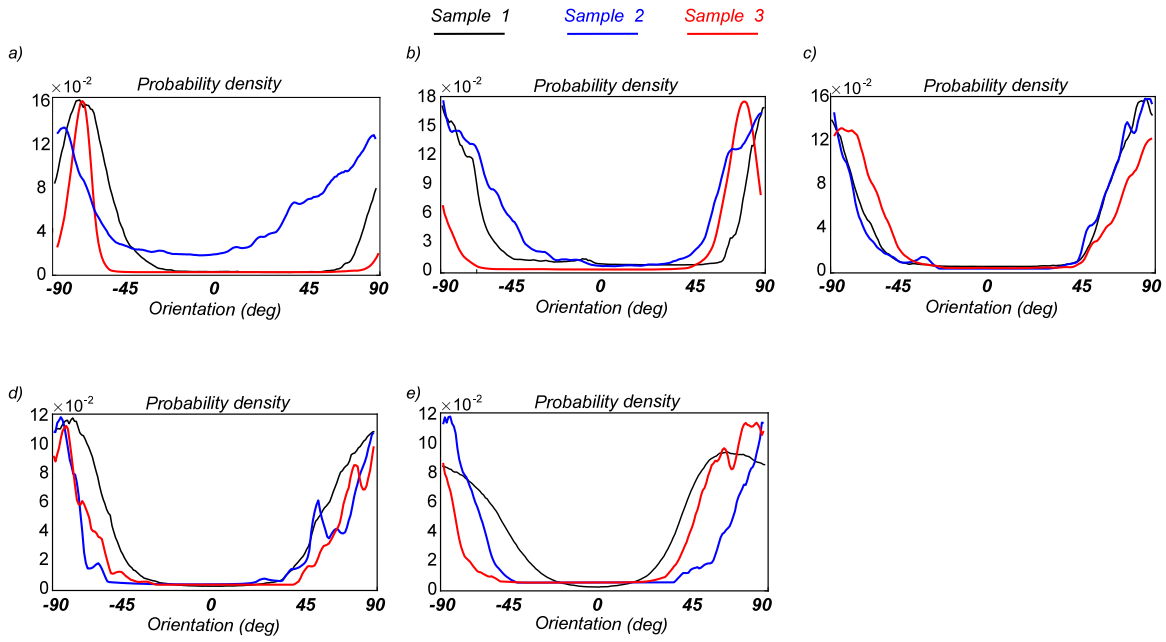

Fig. A.12. Intra specimen fiber morphology variation in Trachealis muscle.

is then computed as shown in Eq. (B.1).

$$\sigma_{composite} = A_{adventitia} * \frac{\sigma_{adventitia}}{A_{total}} + A_{cartilage} * \frac{\sigma_{cartilage}}{A_{total}} + A_{mucosa} * \frac{\sigma_{mucosa}}{A_{total}} \tag{B.1}$$

where

$$\sigma_{adventitia} = \frac{Force_{adventitia}}{A_{adventitia}};$$
$$\sigma_{cartilage} = \frac{Force_{cartilage}}{A_{cartilage}}; \tag{B.2}$$
$$\sigma_{mucosa} = \frac{Force_{mucosa}}{A_{mucosa}}$$

It can be seen in Fig. B.13 that the difference between the two responses is approximately 17%, measured by discretizing both curves with fifty sample points. It is to be noted that the two sets do not correspond to the same location, possibly contributing to the difference in the observed response. The comparison however shows the feasibility of using layer specific material models to simulate the tissue's mechanical behavior.

Appendix C. Supplementary data

Supplementary material related to this article can be found online at https://doi.org/10.1016/j.jmbbm.2022.105371.

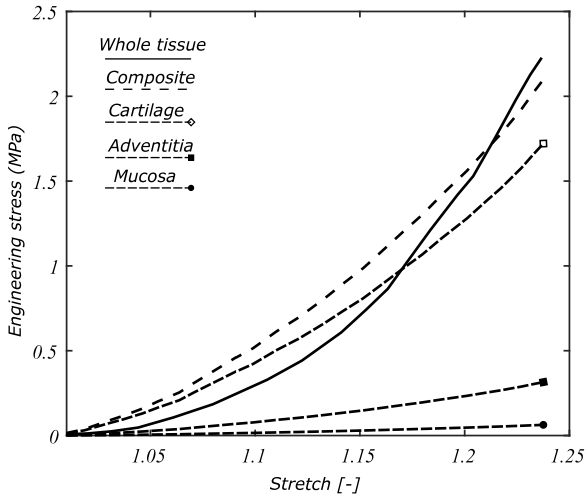

Fig. B.13. Mechanical response comparison of whole tissue vs composite of tissue components.

References

Amiri, M.H., Gabella, G., 1988. Structure of the guinea-pig trachea at rest and in contraction. Anatomy Embryol. 178 (5), 389–397.

Ansari, R., Buj, C., Pieper, M., König, P., Schweikard, A., Hüttmann, G., 2015. Micro-anatomical and functional assessment of ciliated epithelium in mouse trachea using optical coherence phase microscopy. Opt. Express 23 (18), 23217–23224.

Balakrishnan, S., Bu, R., Iftimia, N., Price, H., Zdanski, C., Oldenburg, A.L., 2018. Combined anatomical optical coherence tomography and intraluminal pressure reveal viscoelasticity of the in vivo airway. J. Biomed. Opt. 23 (10), 100501.

Benjamin, B., Pitkin, J., Cohen, D., 1981. Congenital tracheal stenosis. Ann. Otol. Rhinol. Laryngol. 90 (4), 364–371.

Bhutani, V.K., Rubenstein, S.D., Shaffer, T.H., 1981. Pressure-volume relationships of tracheae in fetal newborn and adult rabbits. Resp. Physiol. 43 (3), 221–231.

Boazak, E.M., Auguste, D.T., 2018. Trachea mechanics for tissue engineering design. ACS Biomater. Sci. Eng. 4 (4), 1272–1284.

Brockbank, K.G., MacLellan, W.R., Xie, J., Hamm-Alvarez, S.F., Chen, Z.Z., Schenke-Layland, K., 2008. Quantitative second harmonic generation imaging of cartilage damage. Cell Tissue Bank. 9 (4), 299–307.

Butler, B., Bo, C., Tucker, A., Jardine, A., Proud, W., Williams, A., Brown, K., 2014. Mechanical and histological characterization of trachea tissue subjected to blast-type pressures. In: J. Phys. Conf. Ser.. 500 (18), 182007, IOP Publishing.

Chandran, P.L., Barocas, V.H., 2006. Affine versus non-affine fibril kinematics in collagen networks: theoretical studies of network behavior.

Choudhury, N., Bouchot, O., Rouleau, L., Tremblay, D., Cartier, R., Butany, J., Mongrain, R., Leask, R.L., 2009. Local mechanical and structural properties of healthy and diseased human ascending aorta tissue. Cardiovasc. Pathol. 18 (2), 83–91.

Cinar, U., Halezeroglu, S., Okur, E., Inanici, M.A., Kayaoglu, S., 2016. Tracheal length in adult human: the results of 100 autopsies. Int. J. Morphol. 34, 232–236.

Cova, M., Toffanin, R., 2002. MR microscopy of hyaline cartilage: current status. Eur. Radiol. 12 (4), 814–823.

Croteau, J.R., Cook, C.D., 1961. Volume-pressure and length-tension measurements in human tracheal and bronchial segments. J. Appl. Physiol. 16 (1), 170–172.

Cyron, C., Humphrey, J., 2017. Growth and remodeling of load-bearing biological soft tissues. Meccanica 52 (3), 645–664.

D'Amore, A., Amoroso, N., Gottardi, R., Hobson, C., Carruthers, C., Watkins, S., Wagner, W.R., Sacks, M.S., 2014. From single fiber to macro-level mechanics: a structural finite-element model for elastomeric fibrous biomaterials. J. Mech. Behav. Biomed. Mater. 39, 146–161.

Doeing, D.C., Solway, J., 2013. Airway smooth muscle in the pathophysiology and treatment of asthma. J. Appl. Physiol. 114 (7), 834–843.

Downey, R.P., Samra, N.S., 2020. Anatomy, thorax, tracheobronchial tree. StatPearls [Internet].

Eichaker, L., Li, C., King, N., Pepper, V., Best, C., Onwuka, E., Heuer, E., Zhao, K., Grischkan, J., Breuer, C., et al., 2018. Quantification of tissue-engineered trachea performance with computational fluid dynamics. Laryngoscope 128 (8), E273–E280.

Eskandari, M., Arvayo, A.L., Levenston, M.E., 2018. Mechanical properties of the airway tree: heterogeneous and anisotropic pseudoelastic and viscoelastic tissue responses. J. Appl. Physiol. 125 (3), 878–888.

Eskandari, M., Nordgren, T.M., O'Connell, G.D., 2019. Mechanics of pulmonary airways: linking structure to function through constitutive modeling, biochemistry, and histology. Acta Biomater. 97, 513–523.

Fagerholt, E., Børvik, T., Hopperstad, O., 2013. Measuring discontinuous displacement fields in cracked specimens using digital image correlation with mesh adaptation and crack-path optimization. Opt. Lasers Eng. 51 (3), 299–310.

Fraga, J.C., Jennings, R.W., Kim, P.C., 2016. Pediatric tracheomalacia. In: Seminars in Pediatric Surgery, Vol. 25. Elsevier, pp. 156–164.

Frank, M.B.-O., Niestrawska, J., Holzapfel, G., Debotton, G., 2019. Micromechanically-motivated analysis of fibrous tissue. J. Mech. Behav. Biomed. Mater. 96, 69–78.

Gartner, L.P., Hiatt, J.L., 2006. Color Textbook of Histology E-Book. Elsevier Health Sciences.

Gasser, T.C., Ogden, R.W., Holzapfel, G.A., 2006. Hyperelastic modelling of arterial layers with distributed collagen fibre orientations. J. R. Soc. Interface 3 (6), 15–35.

Giraudet, C., Diaz, J., Le Tallec, P., Allain, J.-M., 2022. Multiscale mechanical model based on patient-specific geometry: application to early keratoconus development. J. Mech. Behav. Biomed. Mater. 129, 105121.

Hakansson, C., Toremalm, N., 1968. XXVI studies on the physiology of the trachea: V. Histology and mechanical activity of the smooth muscles. Ann. Otol. Rhinol. Laryngol. 77 (2), 255–263.

Han, H., Fung, Y., 1991. Residual strains in porcine and canine trachea. J. Biomech. 24 (5), 307–315.

Herbert, R.D., Gandevia, S.C., 2019. The passive mechanical properties of muscle.

Ho, A.S., Koltai, P.J., 2008. Pediatric tracheal stenosis. Otolaryngol. Clin. North Amer. 41 (5), 999–1021.

Holzapfel, G.A., Niestrawska, J.A., Ogden, R.W., Reinisch, A.J., Schriefl, A.J., 2015. Modelling non-symmetric collagen fibre dispersion in arterial walls. J. R. Soc. Interface 12 (106), 20150188.

Holzapfel, G.A., Sommer, G., Gasser, C.T., Regitnig, P., 2005. Determination of layer-specific mechanical properties of human coronary arteries with nonatherosclerotic intimal thickening and related constitutive modeling. Amer. J. Physiol. Heart Circul. Physiol. 289 (5), H2048–H2058.

Hysinger, E.B., Panitch, H.B., 2016. Paediatric tracheomalacia. Paediatric Respiratory Rev. 17, 9–15.

Jayyosi, C., Affagard, J.-S., Ducourthial, G., Bonod-Bidaud, C., Lynch, B., Bancelin, S., Ruggiero, F., Schanne-Klein, M.-C., Allain, J.-M., Bruyère-Garnier, K., et al., 2017. Affine kinematics in planar fibrous connective tissues: an experimental investigation. Biomech. Model. Mechanobiol. 16 (4), 1459–1473.

Jeffrey, D., Watt, I., 2003. Imaging hyaline cartilage. British J. Radiol. 76 (911), 777–787.

Kamel, K.S., Beckert, L.E., Stringer, M.D., 2009. Novel insights into the elastic and muscular components of the human trachea. Clin. Anatomy 22 (6), 689–697.

Ke, M.-T., Imai, T., 2014. Optical clearing of fixed brain samples using SeeDB. Curr. Protocols Neurosci. 66 (1), 2–22.

Keyes, J.T., Haskett, D.G., Utzinger, U., Azhar, M., Vande Geest, J.P., 2011. Adaptation of a planar microbiaxial optomechanical device for the tubular biaxial microstructural and macroscopic characterization of small vascular tissues. J. Biomech. Eng..

Kojima, K., Bonassar, L.J., Ignotz, R.A., Syed, K., Cortiella, J., Vacanti, C.A., 2003. Comparison of tracheal and nasal chondrocytes for tissue engineering of the trachea. Annals Thoracic Surg. 76 (6), 1884–1888.

Kojima, K., Vacanti, C.A., 2014. Tissue engineering in the trachea. Anatomical Record 297 (1), 44–50.

Kovanen, V., Suominen, H., Heikkinen, E., 1984. Collagen of slow twitch and fast twitch muscle fibres in different types of rat skeletal muscle. Eur. J. Appl. Physiol. Occupat. Physiol. 52 (2), 235–242.

Krasny, W., Magoariec, H., Morin, C., Avril, S., 2018. Kinematics of collagen fibers in carotid arteries under tension-inflation loading. J. Mech. Behav. Biomed. Mater. 77, 718–726.

Liu, Z., Wang, Y., Teng, Z., Xu, G., Tang, W., 2002. Opening angles and residual strains in normal rat trachea. Sci. China Ser. C 45 (2), 138–148.

Liu, L., Wu, W., Tuo, X., Geng, W., Zhao, J., Wei, J., Yan, X., Yang, W., Li, L., Chen, F., 2010. Novel strategy to engineer trachea cartilage graft with marrow mesenchymal stem cell macroaggregate and hydrolyzable scaffold. Artif. Organs 34 (5), 426–433.

Macleod, L.J., Heard, B., 1969. Area of muscle in tracheal sections in chronic? Bronchitis, measured by point-counting. J. Pathol. 97 (1), 157–161.

Malvè, M., del Palomar, A.P., Mena, A., Trabelsi, O., López-Villalobos, J., Ginel, A., Panadero, F., Doblaré, M., 2011. Numerical modeling of a human stented trachea under different stent designs. Int. Commun. Heat Mass Transfer 38 (7), 855–862.

Meador, W.D., Mathur, M., Sugerman, G.P., Jazwiec, T., Malinowski, M., Bersi, M.R., Timek, T.A., Rausch, M.K., 2020. A detailed mechanical and microstructural analysis of ovine tricuspid valve leaflets. Acta Biomater. 102, 100–113.

Miller, W.S., 1913. The trachealis muscle. its arrangement at the carina tracheae and its probable influence on the lodgment of foreign bodies in the right bronchus and lung. Anatomical Record 7 (11), 373–385.

Mimouni-Benabu, O., Meister, L., Giordano, J., Fayoux, P., Loundon, N., Triglia, J.M., Nicollas, R., 2012. A preliminary study of computer assisted evaluation of congenital tracheal stenosis: A new tool for surgical decision-making. Int. J. Pediatric Otorhinol. 76 (11), 1552–1557.

Minnich, D.J., Mathisen, D.J., 2007. Anatomy of the trachea, carina, and bronchi. Thoracic Surgery Clin. 17 (4), 571–585.

Morin, C., Avril, S., Hellmich, C., 2018. Non-affine fiber kinematics in arterial mechanics: a continuum micromechanical investigation. ZAMM-J. Appl. Math. Mech. Z. Angew. Math. Mech. 98 (12), 2101–2121.

Mortola, J., Sant'Ambrogio, G., 1979. Mechanics of the trachea and behaviour of its slowly adapting stretch receptors. J. Physiol. 286 (1), 577–590.

Nemavhola, F., Ngwangwa, H., Pandelani, T., 2021. Experimental analysis and biaxial biomechanical behaviour of ex-vivo sheep trachea. BioRxiv.

Odin, C., Guilbert, T., Alkilani, A., Boryskina, O.P., Fleury, V., Le Grand, Y., 2008. Collagen and myosin characterization by orientation field second harmonic microscopy. Opt. Express 16 (20), 16151–16165.

Orlando, G., Wood, K.J., Stratta, R.J., Yoo, J.J., Atala, A., Soker, S., 2011. Regenerative medicine and organ transplantation: past, present, and future. Transplantation 91 (12), 1310–1317.

Ott, L.M., Weatherly, R.A., Detamore, M.S., 2011. Overview of tracheal tissue engineering: clinical need drives the laboratory approach. Ann. Biomed. Eng. 39 (8), 2091–2113.

Pasta, S., Phillippi, J.A., Tsamis, A., D'Amore, A., Raffa, G.M., Pilato, M., Scardulla, C., Watkins, S.C., Wagner, W.R., Gleason, T.G., et al., 2016. Constitutive modeling of ascending thoracic aortic aneurysms using microstructural parameters. Med. Eng. Phys. 38 (2), 121–130.

Peddada, S.D., Haseman, J.K., 2005. Analysis of nonlinear regression models: a cautionary note. Dose-Response 3 (3), dose–response.

Perrin, D., Badel, P., Orgéas, L., Geindreau, C., Dumenil, A., Albertini, J.-N., Avril, S., 2015. Patient-specific numerical simulation of stent-graft deployment: Validation on three clinical cases. J. Biomech. 48 (10), 1868–1875.

Polzer, S., Gasser, T.C., Forsell, C., Druckmüllerova, H., Tichy, M., Staffa, R., Vlachovsky, R., Bursa, J., 2013. Automatic identification and validation of planar collagen organization in the aorta wall with application to abdominal aortic aneurysm. Microsc. Microanal. 19 (6), 1395–1404.

Rains, J., Bert, J., Roberts, C., Pare, P., 1992. Mechanical properties of human tracheal cartilage. J. Appl. Physiol. 72 (1), 219–225.

Rezakhaniha, R., Agianniotis, A., Schrauwen, J.T.C., Griffa, A., Sage, D., Bouten, C.v., Van De Vosse, F., Unser, M., Stergiopulos, N., 2012. Experimental investigation of collagen waviness and orientation in the arterial adventitia using confocal laser scanning microscopy. Biomech. Model. Mechanobiol. 11 (3), 461–473.

Robertson, C., Chen, Z., George, S.C., Lee, S.-W., Ahn, Y.-C., Mahon, S., Brenner, M., 2011. Investigating in vivo airway wall mechanics during tidal breathing with optical coherence tomography. J. Biomed. Opt. 16 (10), 106011.

Sadeghinia, M.J., Skallerud, B., Holzapfel, G.A., Prot, V., 2022. Biomechanics of mitral valve leaflets: Second harmonic generation microscopy, biaxial mechanical tests and tissue modeling. Acta Biomater..

Safshekan, F., Tafazzoli-Shadpour, M., Abdouss, M., Shadmehr, M.B., Ghorbani, F., 2017. Investigation of the mechanical properties of the human tracheal cartilage. Tanaffos 16 (2), 107.

Safshekan, F., Tafazzoli-Shadpour, M., Abdouss, M., Shadmehr, M.B., Ghorbani, F., 2020. Finite element simulation of human trachea: normal vs. surgically treated and scaffold implanted cases. Int. J. Solids Struct. 190, 35–46.

Safshekan, M.B., 2016. Mechanical characterization and constitutive modeling of human trachea age and gender dependency. Materials 9 (6), 456.

Sun, Q., Tiziana, P., Khan, A.u.M., Heuveline, V., Gretz, N., 2021. A simple optical tissue clearing pipeline for 3D vasculature imaging of the mediastinal organs in mice. Int. J. Exp. Pathol. 102 (4–5), 218–227.

Teng, Z., Liu, Z., Lin, Y., Wang, Y., Li, F., Gong, K., 2004. Study on cartilaginous and muscular strains of rat trachea. Sci. China Ser. C 47 (6), 485–493.

Teng, Z., Ochoa, I., Li, Z., Lin, Y., Rodriguez, J.F., Bea, J.A., Doblare, M., 2008. Nonlinear mechanical property of tracheal cartilage: a theoretical and experimental study. J. Biomech. 41 (9), 1995–2002.

Teng, Z., Trabelsi, O., Ochoa, I., He, J., Gillard, J.H., Doblare, M., 2012. Anisotropic material behaviours of soft tissues in human trachea: an experimental study. J. Biomech. 45 (9), 1717–1723.

Terzolo, A., Bailly, L., Orgéas, L., Cochereau, T., Bernardoni, N.H., 2022. A micromechanical model for the fibrous tissues of vocal folds. J. Mech. Behav. Biomed. Mater. 128, 105118.

Thiberville, L., Moreno-Swirc, S., Vercauteren, T., Peltier, E., Cavé, C., Bourg Heckly, G., 2007. In vivo imaging of the bronchial wall microstructure using fibered confocal fluorescence microscopy. Am. J. Respir. Crit. Care Med. 175 (1), 22–31.

Tiaho, F., Recher, G., Rouède, D., 2007. Estimation of helical angles of myosin and collagen by second harmonic generation imaging microscopy. Opt. Express 15 (19), 12286–12295.

Trabelsi, O., Del Palomar, A.P., López-Villalobos, J., Ginel, A., Doblaré, M., 2010. Experimental characterization and constitutive modeling of the mechanical behavior of the human trachea. Med. Eng. Phys. 32 (1), 76–82.

Young, C.D., Moore, G.W., Hutchins, G.M., 1980. Connective tissue arrangement in respiratory airways. Anatomical Record 198 (2), 245–254.

Zhu, X., Liao, C., Wang, Z., Zhuo, S., Liu, W., Chen, J., 2016. Quantification of collagen distributions in rat hyaline and fibro cartilages based on second harmonic generation imaging. In: Optics in Health Care and Biomedical Optics VII, Vol. 10024. International Society for Optics and Photonics, 1002424.